63. Chong, J.M.; Sakuma, K.; Sudo, M.; Ushiku, T.; Uozaki, H.; Shibahara, J.; Nagai, H.; Funata, N.; Taniguchi, H.; Aburatani, H.; *et al.* Global and non-random CpG-island methylation in gastric carcinoma associated with Epstein-Barr virus. *Cancer Sci.* **2003**, *94*, 76–80.
64. Feng, W.H.; Hong, G.; Delecluse, H.J.; Kenney, S.C. Lytic induction therapy for Epstein-Barr virus-positive B-cell lymphomas. *J. Virol.* **2004**, *78*, 1893–1902.
65. Saito, M.; Nishikawa, J.; Okada, T.; Morishige, A.; Sakai, K.; Nakamura, M.; Kiyotoki, S.; Hamabe, K.; Okamoto, T.; Oga, A.; *et al.* Role of DNA methylation in the development of Epstein-Barr virus-associated gastric carcinoma. *J. Med. Virol.* **2013**, *85*, 121–127.
66. Okada, T.; Nakamura, M.; Nishikawa, J.; Sakai, K.; Zhang, Y.; Saito, M.; Morishige, A.; Oga, A.; Sasaki, K.; Suehiro, Y.; *et al.* Identification of genes specifically methylated in Epstein-Barr virus-associated gastric carcinomas. *Cancer Sci.* **2013**, *104*, 1309–1314.
67. Hino, R.; Uozaki, H.; Murakami, N.; Ushiku, T.; Shinozaki, A.; Ishikawa, S.; Morikawa, T.; Nakaya, T.; Sakatani, T.; Takada, K.; *et al.* Activation of DNA methyltransferase 1 by EBV latent membrane protein 2A leads to promoter hypermethylation of PTEN gene in gastric carcinoma. *Cancer Res.* **2009**, *69*, 2766–2774.
68. Luo, B.; Wang, Y.; Wang, X.F.; Liang, H.; Yan, L.P.; Huang, B.H.; Zhao, P. Expression of Epstein-Barr virus genes in EBV-associated gastric carcinomas. *World J. Gastroenterol.* **2005**, *11*, 629–633.
69. Lennette, E.T.; Winberg, G.; Yadav, M.; Enblad, G.; Klein, G. Antibodies to LMP2A/2B in EBV-carrying malignancies. *Eur. J. Cancer* **1995**, *31A*, 1875–1878.
70. Tsai, C.L.; Li, H.P.; Lu, Y.J.; Hsueh, C.; Liang, Y.; Chen, C.L.; Tsao, S.W.; Tse, K.P.; Yu, J.S.; Chang, Y.S. Activation of DNA methyltransferase1 by EBV LMP1 Involves *c*-Jun NH(2)-terminal kinase signaling. *Cancer Res.* **2006**, *66*, 11668–11676.
71. Tsai, C.N.; Tsai, C.L.; Tse, K.P.; Chang, H.Y.; Chang, Y.S. The Epstein-Barr virus oncogene product, latent membrane protein 1, induces the downregulation of E-cadherin gene expression via activation of DNA methyltransferases. *Proc. Natl. Acad. Sci. USA* **2002**, *99*, 10084–10089.
72. Kida, Y.; Miyauchi, K.; Takano, Y. Gastric adenocarcinoma with differentiation to sarcomatous components associated with monoclonal Epstein-Barr virus infection and LMP-1 expression. *Virchows Archiv. A Pathol. Anat. Histopathol.* **1993**, *423*, 383–387.
73. Kanai, Y.; Hui, A.M.; Sun, L.; Ushijima, S.; Sakamoto, M.; Tsuda, H.; Hirohashi, S. DNA hypermethylation at the D17S5 locus and reduced HIC-1 mRNA expression are associated with hepatocarcinogenesis. *Hepatology* **1999**, *29*, 703–709.
74. Kondo, Y.; Kanai, Y.; Sakamoto, M.; Mizokami, M.; Ueda, R.; Hirohashi, S. Genetic instability and aberrant DNA methylation in chronic hepatitis and cirrhosis—A comprehensive study of loss of heterozygosity and microsatellite instability at 39 loci and DNA hypermethylation on 8 CpG islands in microdissected specimens from patients with hepatocellular carcinoma. *Hepatology* **2000**, *32*, 970–979.
75. Niller, H.H.; Wolf, H.; Minarovits, J. Epigenetic dysregulation of the host cell genome in Epstein-Barr virus-associated neoplasia. *Semin. Cancer Biol.* **2009**, *19*, 158–164.
76. Masucci, M.G.; Contreras-Salazar, B.; Ragnar, E.; Falk, K.; Minarovits, J.; Ernberg, I.; Klein, G. 5-Azacytidine up regulates the expression of Epstein-Barr virus nuclear antigen 2 (EBNA-2)

through EBNA-6 and latent membrane protein in the Burkitt's lymphoma line rael. *J. Virol.* **1989**, *63*, 3135–3141.

77. Ernberg, I.; Falk, K.; Minarovits, J.; Busson, P.; Tursz, T.; Masucci, M.G.; Klein, G. The role of methylation in the phenotype-dependent modulation of Epstein-Barr nuclear antigen 2 and latent membrane protein genes in cells latently infected with Epstein-Barr virus. *J. Gen. Virol.* **1989**, *70*, 2989–3002.
78. Hu, L.F.; Minarovits, J.; Cao, S.L.; Contreras-Salazar, B.; Rymo, L.; Falk, K.; Klein, G.; Ernberg, I. Variable expression of latent membrane protein in nasopharyngeal carcinoma can be related to methylation status of the Epstein-Barr virus BNLF-1 5'-flanking region. *J. Virol.* **1991**, *65*, 1558–1567.
79. Iwakiri, D.; Eizuru, Y.; Tokunaga, M.; Takada, K. Autocrine growth of Epstein-Barr virus-positive gastric carcinoma cells mediated by an Epstein-Barr virus-encoded small RNA. *Cancer Res.* **2003**, *63*, 7062–7067.
80. Nanbo, A.; Yoshiyama, H.; Takada, K. Epstein-Barr virus-encoded poly(A)-RNA confers resistance to apoptosis mediated through Fas by blocking the PKR pathway in human epithelial intestine 407 cells. *J. Virol.* **2005**, *79*, 12280–12285.
81. Seto, E.; Yang, L.; Middeldorp, J.; Sheen, T.S.; Chen, J.Y.; Fukayama, M.; Eizuru, Y.; Ooka, T.; Takada, K. Epstein-Barr virus (EBV)-encoded BARF1 gene is expressed in nasopharyngeal carcinoma and EBV-associated gastric carcinoma tissues in the absence of lytic gene expression. *J. Med. Virol.* **2005**, *76*, 82–88.
82. Hino, R.; Uozaki, H.; Inoue, Y.; Shintani, Y.; Ushiku, T.; Sakatani, T.; Takada, K.; Fukayama, M. Survival advantage of EBV-associated gastric carcinoma: Survivin up-regulation by viral latent membrane protein 2A. *Cancer Res.* **2008**, *68*, 1427–1435.
83. Wiech, T.; Nikolopoulos, E.; Lassman, S.; Heidt, T.; Schöpflin, A.; Sarbia, M.; Werner, M.; Shimizu, Y.; Sakka, E.; Ooka, T.; *et al.* Cyclin D1 expression is induced by viral BARF1 and is overexpressed in EBV-associated gastric cancer. *Virchows Arch.* **2008**, *452*, 621–627.
84. Fukuda, M.; Longnecker, R. Latent membrane protein 2A inhibits transforming growth factor-beta 1-induced apoptosis through the phosphatidylinositol 3-kinase/Akt pathway. *J Virol.* **2004**, *78*, 1697–1705.
85. Bartel, D.P. MicroRNAs: Target recognition and regulatory functions. *Cell* **2009**, *136*, 215–233.
86. Lung, R.W.; Tong, J.H.; To, K.F. Emerging roles of small Epstein-Barr virus derived non-coding RNAs in epithelial malignancy. *Int. J. Mol. Sci.* **2013**, *14*, 17378–17409.
87. Lung, R.W.; Tong J.H.; Sung, Y.M.; Leung, P.S.; Ng, D.C.; Chau, S.L.; Chan, A.W.; Ng, E.K.; Lo, K.W.; To, K.F. Modulation of LMP2A expression by a newly identified Epstein-Barr virus-encoded microRNA miR-BART22. *Neoplasia* **2009**, *11*, 1174–1184.
88. Iizasa, H.; Nanbo, A.; Nishikawa, J.; Jinushi, M.; Yoshiyama, H. Epstein-Barr Virus (EBV)-associated gastric carcinoma. *Viruses* **2012**, *4*, 3420–3439.
89. Iizasa, H.; Wulff, B.E.; Alla, N.R.; Maragkakis, M.; Megraw, M.; Hatzigeorgiou, A.; Iwakiri, D.; Takada, K.; Wiedmer, A.; Showe, L.; *et al.* Editing of Epstein-Barr virus-encoded BART6 microRNAs controls their dicer targeting and consequently affects viral latency. *J. Biol. Chem.* **2010**, *285*, 33358–33370.

90. Choy, E.Y.; Siu, K.L.; Kok, K.H.; Lung, R.W.; Tsang, C.M.; To, K.F.; Kwong, D.L.; Tsao, S.W.; Jin, D.Y. An Epstein-Barr virus-encoded microRNA targets PUMA to promote host cell survival. *J. Exp. Med.* **2008**, *205*, 2551–2560.
91. Choi, H.; Lee, H.; Kim, S.R.; Gho, Y.S.; Lee, S.K. Epstein-Barr virus-encoded microRNA BART15-3p promotes cell apoptosis partially by targeting BRUCE. *J. Virol.* **2013**, *87*, 8135–8144.
92. Qiu, J.; Cosmopoulos, K.; Pegtel, M.; Hopmans, E.; Murray, P.; Middeldorp, J.; Shapiro, M.; Thorley-Lawson, D.A. A novel persistence associated EBV miRNA expression profile is disrupted in neoplasia. *PLoS Pathog.* **2011**, *7*, e1002193.
93. Marquitz, A.R.; Mathur, A.; Chugh, P.E.; Dittmer, D.P.; Raab-Traub, N. Expression profile of microRNAs in Epstein-Barr virus-infected AGS gastric carcinoma cells. *J. Virol.* **2014**, *88*, 1389–1393.
94. Kim, D.N.; Chae, H.S.; Oh, S.T.; Kang, J.H.; Park, C.H.; Park, W.S.; Takada, K.; Lee, J.M.; Lee, W.K.; Lee, S.K. Expression of viral microRNAs in Epstein-Barr virus-associated gastric carcinoma. *J. Virol.* **2007**, *81*, 1033–1036.
95. Kim, D.N.; Lee, S.K. Biogenesis of Epstein-Barr virus microRNAs. *Mol. Cell. Biochem.* **2012**, *365*, 203–210.
96. Kim, D.N.; Seo, M.K.; Choi, H.; Kim, S.Y.; Shin, H.J.; Yoon, A.R.; Tao, Q.; Rha, S.Y.; Lee, S.K. Characterization of naturally Epstein-Barr virus-infected gastric carcinoma cell line YCCEL1. *J. Gen. Virol.* **2013**, *94*, 497–506.

J Infect Chemother 20 (2014) 169–174

Contents lists available at ScienceDirect

Journal of Infection and Chemotherapy

journal homepage: http://www.elsevier.com/locate/jic

Original article

Colonization of an acid resistant *Kingella denitrificans* in the stomach may contribute to gastric dysbiosis by *Helicobacter pylori*

Takeshi Okamoto [a,1], Yasuhiro Hayashi [b,1], Hidekazu Mizuno [c], Hideo Yanai [d], Jun Nishikawa [a], Teruko Nakazawa [a], Hisashi Iizasa [b], Masahisa Jinushi [b], Isao Sakaida [a], Hironori Yoshiyama [b,*]

[a] *Yamaguchi University, Graduate School of Medicine, Minamikogushi 1-1-1, Ube, Yamaguchi 755-8505, Japan*
[b] *Institute for Genetic Medicine, Hokkaido University, N15 W7, Kita-ku, Sapporo, Hokkaido 060-0815, Japan*
[c] *Clinical Laboratory, Yamaguchi University Hospital, Minamikogushi 1-1-1, Ube, Yamaguchi 755-8505, Japan*
[d] *Department of Clinical Research, National Hospital Organization Kanmon Medical Center, 1-1 Sotoura, Chofu, Shimonoseki, Yamaguchi 752-8510, Japan*

ARTICLE INFO

Article history:
Received 19 June 2013
Received in revised form
4 September 2013
Accepted 16 September 2013

Keywords:
Anti-acid administration
Gastric barrier to bacteria
Helicobacter pylori
Kingella denitrificans
Dysbiosis

ABSTRACT

In the stomach of a gastric ulcer patient who had been administered an anti-acid, a gram-negative and urease-negative bacillus similar in size to *Helicobacter pylori* was infected together with *H. pylori*. According to biochemical test and 16S rRNA gene analysis, the urease-negative bacterium was identified as *Kingella denitrificans*, a human nasopharyngeal commensal. In contrast to the standard strain of *K. denitrificans*, the isolate showed catalase activity, did not produce acid from glucose, and exhibited acid tolerance. Acid tolerance of *H. pylori* was increased by cocultivation with the *K. denitrificans* isolate, but not with other isolates of *K. denitrificans*. Disruption of physiological and immunological niche by dysbiotic colonization of bacterium may provide pathological attributes to human stomach. Collectively, a careful administration of anti-acids to the elderly, especially those with atrophic gastritis, is necessary to avoid repression of the gastric barrier to bacteria.

1. Introduction

Helicobacter pylori (*H. pylori*) colonizes approximately half of the world's population and causes chronic gastritis, peptic ulcers, and gastric adenocarcinoma [1]. Eradication of this bacterium improves the symptoms of patients with peptic ulcer and gastric lymphoma of mucosa-associated lymphoid tissue [2,3]. Isolation of *H. pylori* from endoscopic gastric biopsy specimens is the most reliable method for detecting *H. pylori* infection and essential for drug susceptibility testing [4].

The gastric acid determines bacterial susceptibility to the stomach and inhibits infectious agents from reaching the intestine [5]. Urease activity is crucial for *H. pylori* to colonize the stomach through neutralizing the acidic environment and providing chemotactic motility [6]. However, colonization of urease-negative *H. pylori* and *Campylobacter jejuni* is reported in patients receiving acid-reducing compounds [7,8]. Moreover, predisposed decrease of acid secretion, due to therapy, disease, or age, increased bacterial population in gastric juice [9,10]. Disproportional use of proton pump inhibitors is considered to promote small intestinal bacterial overgrowth, which is prevalent in patients with irritable bowel disease (IBD) [11]. The gastrointestinal microbiota clearly contributes to development of IBD both in mouse models and patients [12].

A gram-negative bacillus, *Kingella denitrificans* (*K. denitrificans*), is a component of the normal upper respiratory and genitourinary tract flora and sometimes causes severe infection [13–15]. *Kingella* species are plump gram-negative bacilli and positive for cytochrome *c* oxidase [16]. Unlike the related species, such as *Neisseriae* and *Moraxellae*, *Kingella* species are catalase-negative similar to *Cardiobacterium hominis* and *Eikenella corrodens*. However, strain UB-75 of *Kingella oralis* and strain UB-204 of *E. corrodens* were catalase positive [17]. The type-strain of *K. denitrificans* characteristically produces acid from glucose and is positive for prolyl-aminopeptidase. Different from other species in the genus, *K. denitrificans* reduces nitrate to nitrite [16].

Necessity for careful identification of urease-negative bacteria in the gastric mucosa is highlighted in this paper. Of particular

* Corresponding author. Present address: Shimane University, Faculty of Medicine, Enyacho 89-1, Izumo, Shimane 693-8501, Japan. Tel.: +81 853 20 2148; fax: +81 853 20 2147.
E-mail address: yosiyama@med.shimane-u.ac.jp (H. Yoshiyama).
[1] Two authors contributed equally to the work.

1341-321X/$ – see front matter © 2013, Japanese Society of Chemotherapy and The Japanese Association for Infectious Diseases. Published by Elsevier Ltd. All rights reserved.
http://dx.doi.org/10.1016/j.jiac.2013.09.007

interest, disruption of integrated immunological niche by dysbiotic colonization of commensal bacteria is discussed.

2. Materials and methods

2.1. Patient

A 78-year-old man suffering from gastric ulcer had been administered 40 mg of histamine receptor 2 (H2) antagonist, ranitidine, per day for two years. Endoscopic observation revealed multiple gastric ulcer scars with severe atrophic gastritis. Gastric mucosal biopsy from the antrum and the body was performed to determine histological findings and detect *H. pylori*. The biopsy specimen was positive for the CLO-test (Kimbarly-Clark, Roswell, GA).

The study was approved by the Yamaguchi University Hospital Ethics Committee. Informed consent was obtained from the patient. The research was carried out in accordance with the Declaration of Helsinki.

2.2. Bacterial isolation and culture conditions

The gastric biopsy specimen was homogenized and a loopful of inoculum was streaked onto a plate of an HP selective medium (Eiken Chemical Inc., Tokyo, Japan) containing amphotericin B (2 μg/ml), trimethoprim (5 μg/ml), polymyxin B (2.5 IU/ml), and vancomycin (10 μg/ml). The plate was grown in a microaerobic atmosphere (5% O_2, 10% CO_2, 85% N_2) at 37 °C for 5 days. The type-strain of *K. denitrificans* ATCC33394 was obtained from the American Type Culture Collection. *K. denitrificans* KDY1 was isolated from a nasopharyngeal swab of a leukemic patient and *H. pylori* CPY3401 was from gastric biopsy specimen [18] in Yamaguchi University Hospital, respectively. And HPT73 is an isogenic *ureB*-disrupted mutant of CPY3401. The culture condition of *K. denitrificans* was exactly the same as that of *H. pylori*.

2.3. Morphology

Hematoxylin-eosin, Giemsa, and Gram stainings were performed by a standard method. For electron microscopy, bacteria were grown in brucella broth containing 3% horse serum for 24 h, washed once with 5 volumes of 10% glycerol MOPS buffer and suspended in 5 volumes of saline. Samples were dried onto a collodion-carbon-coated grid. Shadowing was performed and samples were observed with a JEM-200CX (JEOL) transmission electron microscope as described [18].

2.4. Detection of a H. pylori-specific gene in paraffin-embedded biopsy samples

DNA was extracted from paraffin-embedded gastric biopsy tissues using DEXPAD (Takara BioCo. Shiga, Japan) and subjected to PCR. The primers ureF1 (ATA TTA TGG AAG AAG CGA GAG C) and ureR (ATG GAA GTG TGA GCC GAT TTG), corresponding to bases 2783–2804 and 3076–3096, respectively, of the ureA gene of *H. pylori* amplified 314-bp fragments. For the second round of PCR amplification, primers ureR and ureF2 (CAT GAA GTG GGT ATT GAA GC; +2893–2912) were used.

2.5. Biochemical characterization

Catalase production was tested by placing bacteria from the plates into a drop of 3% hydrogen peroxide on a slide glass. Cytochrome *c* oxidase activity was tested on an oxidase strip (Eiken Chemical Inc.). Hydrolysis of urea was detected with Christensen urea agar (Eiken Chemical Inc.).

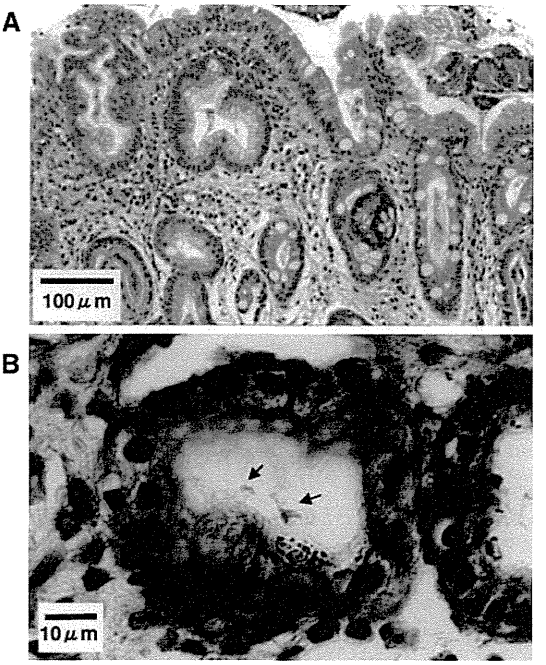

Fig. 1. Histologic section of the biopsy sample. A. The specimen from the antral lesions of chronic active gastritis was stained with hematoxylin and eosin. Infiltration by mononuclear cells and grandular atrophy and intestinal metaplasia could be observed. Magnification, ×140. B. H. pylori-like bacteria were stained with Giemsa in the gastric pit of the same antral biopsy specimen as in panel A. Arrows indicate curved bacilli. Magnification, ×1000.

The ID test HN-20 rapid NISSUI (Nissui Pharmaceutical Co., Tokyo, Japan) was used for identifying *Haemophilus* and *Neisseria* species. This system assays activities for alanine aminopeptidase, alkaline phosphatase, nitrate and nitrite reduction, urease, ornithine decarboxylase, indole production, proline aminopeptidase, glucosidase, γ-glutamyl transpeptidase, and β-galactosidase. This system also examines acid production from glucose, maltose, fructose, mannose, mannitol, trehalose, sucrose, lactose, and xylose.

2.6. 16S ribosomal RNA genome sequencing and data analysis

Bacterial 16S rRNA genes were amplified using universal primers for eubacterial 16S rRNA genes [19]. 16S rRNA sequences were compared by using the Clustal W suite of program [20]. The sequences were between 1467 and 1473 bp long, and the 5′ end was located at position 9 and the 3′ end was position 1482 in the *Escherichia coli* numbering system. A rooted phylogenetic tree [21] has been created.

2.7. Acid sensitivity

The survival of the isolate under different pH conditions [22] was evaluated. Cell suspensions from 48 h cultures were incubated at 37 °C for 1 h with glycine-HCl buffer (pH 2.0), McIlvain's buffer (0.2 M Na_2HPO_4, 0.1 M citric acid, [pH 4.0]), and 0.1 M phosphate buffer (pH 7.0). After incubation, serial 10-fold dilutions of the cell suspensions in 150 mM NaCl were plated onto brucella agar plates containing 3% horse serum and incubated for 72 h at 37 °C to determine CFU.

2.8. Urease assay

Urease activity in bacterium [18] was determined and expressed in micromoles of urea hydrolyzed per minute per milligram of protein in the crude extract.

Table 1
Properties of the isolate, *K. denitrificans*, and *H. pylori*.

	H. pylori CPY3401 Urease (+)	*H. pylori* HPT73 Urease (−)	*K. denitrificans* NHP1	*K. denitrificans* ATCC3394	*K. denitrificans* KDY1
Catalase production[a]	+	+	+	−	−
Oxidase production[a]	+	+	+	+	+
Alanine aminopeptidase	+	+	+	+	+
Phosphatase	−	−	−	−	−
Nitrate reduction	−	−	+	+	+
Nitrite reduction	−	−	+	+	+
Urease activity[a]	+	−	−	−	−
Indole production	−	−	−	−	−
Ornithine decarboxylase	−	−	−	−	−
Glucosidase	−	−	−	−	−
Proline aminopeptidase	−	−	+	+	+
γ-Glutamyl aminopeptidase	+	+	−	−	−
Acid production from					
Glucose	−	−	−	+[b]	+
Maltose	−	−	−	−	−
Fructose	−	−	−	−	−
Mannose	−	−	−	−	−
Mannitol	−	−	−	−	−
Trehalose	−	−	−	−	−
Sucrose	−	−	−	−	−
Lactose	−	−	−	−	−
Xylose	−	−	−	−	−
Growth at 42°	−	−	+	+	+

[a] Items for routine assay to identify *H. pylori*.
[b] Weakly positive.

3. Results

3.1. Isolation of a gram-negative and urease-negative bacterium

The histology of the gastric biopsy specimens indicated granular atrophy and intestinal metaplasia accompanied by infiltration of mononuclear cells to the lamina propria, a typical observation in gastric mucosa infected with *H. pylori* (Fig. 1A). Though it is not specific, a few bacteria-like organisms could be seen in the gastric lumen (Fig. 1B). *H. pylori ureA* gene was amplified in the paraffin-embedded gastric tissue (not shown).

A bacterium isolated from the culture of biopsy specimen was named NHP1. The bacterial colonies corroded the agar surface and had no hemolytic activity on sheep blood agar. Growth was obtained at 37 and 42 °C under the microaerobic conditions (Table 1). A gram-negative bacillus, quite similar in size and morphology with *H. pylori* was observed (Fig. 2). However, NHP1 lacked the urease activity.

3.2. Morphological and genetical analysis

The electron microscopy showed that *H. pylori* CPY3401 had a curved body with a bundle of sheathed flagella at one pole (Fig. 3A), whereas strain NHP1 was rod-shaped with no flagella and sometimes appeared in pairs (Fig. 3B).

The basic local alignment search tool showed that the 16S rRNA sequence of NHP1 had the highest similarity with the gene of *K.*

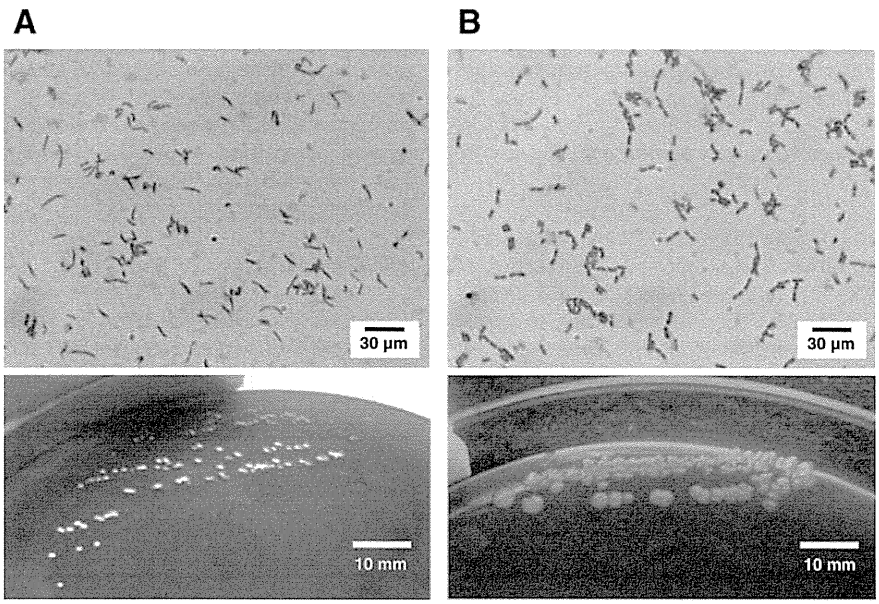

Fig. 2. Gram stain and colonies of bacteria. Bacteria were cultured for 2 days with HP selective plate. The grown bacterial colonies (lower pictures) were smeared on the glass and Gram-stained (upper pictures). A. *H. pylori* CPY3401, B. NHP1, Magnification of Gram Stain, ×1000.

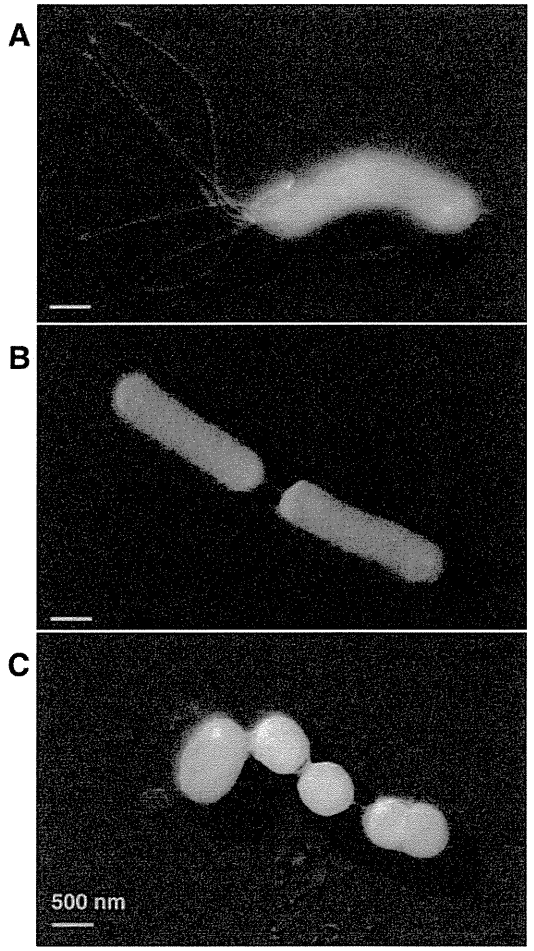

Fig. 3. Electron micrographs. A. *H. pylori* CPY3401, B. NHP1 C. *K. denitrificans* KDY1, Bar = 500 nm.

denitrificans (Fig. 4A). The 1468 sequence alignment of NHP1 and *K. denitrificans* ATCC33394 (type-strain) had 99% identity (not shown). NHP1 differs in its sequence by only 3 bases from UB-294, an oral isolate of *K. denitrificans* [23] and by 5 bases from ATCC33394 (Fig. 4B). Since a phylogenetic tree derived from the distant matrix by using the neighbor joining method [28] formed a tight cluster on the tree (Fig. 4A), NHP1 was diagnosed as *K. denitrificans*.

However, the electronmicrograph of another isolate of *K. denitrificans*, KDY1, was 0.5–0.6 by 0.5–1.0 μm that is shorter than NHP1 and CPY3401 and had long and thin pili about 5 nm in diameter (Fig. 3C). NHP1 resembled to *H. pylori* at a glance especially in size, but *H. pylori* possessed slightly curved body when observed carefully (Fig. 2).

3.3. Biochemical identification

A scoring-based test system for *Haemophilus* and *Neisseria* species showed NHP1 as *K. denitrificans* at the highest probability (12% in Table 1). Since other species name having the similar score was not presented by the ID test, the isolate was identified as *K. denitrificans*. Biochemical features of NHP1 were almost identical to those of *K. denitrificans* strains, ATCC33394 and KDY1, except for catalase activity and acid production from glucose. The scoring system diagnosed the NHP1 isolate as *K. denitrificans*, consistent with the sequencing result.

3.4. Acid sensitivity

The acid sensitivity of *H. pylori* CPY3401 was compared with *K. denitrificans* NHP1, KDY1, and ATCC33394 (Table 2). Colony forming units per ml (CFU/ml) of the initial inoculum of NHP1 numbered $10^{7.9}$, declining to $10^{6.2}$ after a 1 h exposure to pH 4.0 at 37 °C. On the other hand, CFU/ml of the initial inoculum of *H. pylori* CPY3401 numbered $10^{8.2}$, decreasing to $10^{4.1}$ after 1 h at pH 4.0. Thus, the survival ratio of bacteria after 1 h at pH 4.0 was 1 in $10^{1.7}$ in *K. denitrificans* NHP1, compared to 1 in $10^{4.1}$ in *H. pylori*. *K. denitrificans* NHP1 was indicated $10^{2.4}$-fold more tolerant to acid (pH 4.0) than *H. pylori* CPY3401. In contrast, the type-strain (ATCC33394) and a clinical isolate (KDY1) were vulnerable to acid. Their initial inocula numbered $10^{8.3}$ and $10^{7.8}$, respectively, declining to less than $10^{1.0}$ after exposure to pH 4.0.

Each isolate of *K. denitrificans* was mixed one-on-one with *H. pylori* CPY3401 and exposed to buffers with different pH. The initial CFU/ml of *H. pylori* and NHP1 mixture numbered $10^{7.9}$, declining to $10^{6.5}$ after a 1 h exposure to pH 4.0. Five hundred clones were picked up from the colonies exposed to pH 4.0, then subjected to urease assay. The urease activity of *H. pylori* CPY3401 and NHP1 was 353.5 mmol/min/mg and 15.4 mmol/min/mg, respectively. None of the pH 4 plates either from *H. pylori* and ATCC33394 or *H. pylori* and KDY1 showed more than 100 mmol/min/mg of urease activity. On the other hand, number of colonies which showed more than 100 mmol/min/mg of urease activity in the pH 4 plate of the *H. pylori* and NHP1 was 116 (23.2%), indicating CFU/ml of survived *H. pylori* was $10^{6.15}$. When *H. pylori* was mixed with other isolates of *K. denitrificans* (ATCC33394 and KDY1), all of the survived bacteria after exposure to pH 4.0 showed urease activity and CFU/ml did not exceeded 10^4. Acid tolerance of *H. pylori* was increased up to 160-fold by cocultivation with acid tolerant *K. denitrificans* NHP1.

We have repeated the experiment by changing the time length (20, 40, and 60 min) for bacterial exposure to acidic conditions (pH 2, 4, and 7). In the acidic condition (pH 4), single culture of *H. pylori* could not survive. However, mixture of *H. pylori* with *K. denitrificans* showed survival of *H. pylori* after 20 min in pH 4, which was better when mixed with acid tolerant NHP1 (65.4%) than with ATCC33394 (32.1%) (Fig. 5).

4. Discussion

The gastric juice represents a barrier to microbes in saliva and ingested food, mainly by the bactericidal activity of hydrochloric acid [23]. A study in patients with hypochlorhydria being treated with anti-acid and histamine receptor 2 (H2) antagonists identified bacteria originating from the mouth in the gastric contents [24]. Moreover, acid-inhibiting proton pump inhibitors caused gastric colonization by oral-type bacteria in healthy volunteers [10]. The gastric barrier to infection has more significant meaning to hosts having a weakened immunological defense [25].

We isolated a rod-shaped isolate of *K. denitrificans*, which is different from general plump-shaped isolate not only by the morphology. However, the 16S rRNA sequence of the isolate showed 99% identity with the type-strain ATCC33394. The novel *K. denitrificans* isolate, NHP1, was better able to survive in acidic conditions than the type-strain of *K. denitrificans* (Table 2). Though acid exposure of *H. pylori* alone did not show survival of the bacterium, mixture of *H. pylori* with *K. denitrificans* showed survival of *H. pylori* (Fig. 5). We assume that *K. denitrificans* may bind with *H. pylori*, thus, *K. denitrificans* enables *H. pylori* more acid resistant by coating the bacterial body. This coating may be more effective in acid tolerant NHP1 than acid sensitive ATCC43349. Such a difference in acid tolerance between isolates could also be observed in

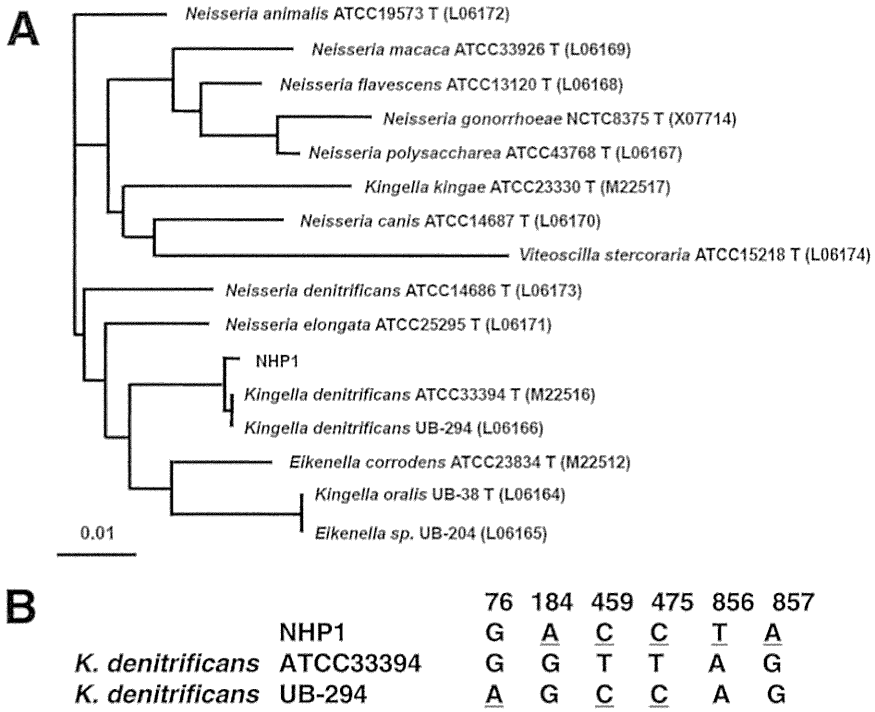

Fig. 4. Genetic analyses of 16S rRNA sequences of *K. denitrificans*. A. Rooted phylogenetic tree based on 16S rRNA sequence comparisons. Bar indicates 0.01% differences in nucleotide sequences. Horizontal distances are equivalent to genetic distances. Type strains are indicated by adding T at the last of each name. 16S rRNA sequences are available for electronic retrieval from GenBank under the accession numbers indicated in each parenthesis. B. Variations of DNA sequences of the 16S rRNA gene of *K. denitrificans*. Numbers are corresponding to positions in the *Escherichia coli* 16S rRNA numbering system. Bases deviated from the sequencing result of type-strain ATCC33394 were underlined.

Neisseria gonorrhoeae [26]. Thus, a specific strain of *K. denitrificans* might be able to survive in the human stomach. Furthermore, *Kingella kingae*, a commensal of the human respiratory tract [27], also causes acute gastroenteritis before the onset of systemic symptoms [28]. Though an association of *K. denitrificans* with gastrointestinal disease has not yet been described, our experimental results showed *K. denitrificans* NHP1 isolate help survive *H. pylori* in the acidic condition.

Human alimentary tract harbors hundreds of commensal microbes that interact with the host and provide genetic, metabolic, and immunological attributes [29]. On the other hand, infection with dysbiotic microbes or environmental stresses such as exposure to xenobiotics could alter compositional or functional properties of gut microbes and disrupt immune homeostasis by specific members of this community [30,31]. Since *K. dentrificans* could be colonized into atrophic gastric epithelium where the mucosal barrier systems are perturbed due to chronic inflammation, it might profoundly affect pathology and clinical prognosis of chronic gastritis caused by *H. pylori* infection. Moreover, the commensal may interact with *H. pylori* to stimulate inflammatory signals that have a great impact on the tumor development and progression [32]. Consistent with this idea, the commensal microbes switch their contribution from gastrointestinal homeostasis to pathogenic inflammation, once they communicate with dysbiotic pathogens such as *Salmonella typhimurium* [33]. Furthermore, it is of great interest to evaluate whether infections with *K. dentrificans* or other commensals are associated with the susceptibility to gastric

Table 2
Survival of bacteria after incubation in solutions of different pH.

	Survival after incubation in buffers[a]		
	pH 2	pH 4	pH 7
Strain			
H. pylori CPY3401	<1.0	4.1	8.2
K. denitrificans NHP1	<1.0	6.2	7.9
K. denitrificans ATCC33394	<1.0	<1.0	8.3
K. denitrificans KDY1	<1.0	<1.0	7.8
Strains			
NHP1 + *H. pylori* CPY3401	<1.0	6.5(6.15)[b]	7.9
ATCC33394 + *H. pylori* CPY3401	<1.0	3.9[c]	7.8
KDY1 + *H. pylori* CPY3401	<1.0	4.0[c]	7.9

[a] Numbers are expressed as log10 CFU/ml of the mean results of more than two experiments.
[b] Since 23.2% of the colonies were positive for urease. log10 CFU/ml of *H. pylori* is 6.15, which is shown in the parenthesis.
[c] All the colonies are urease positive.

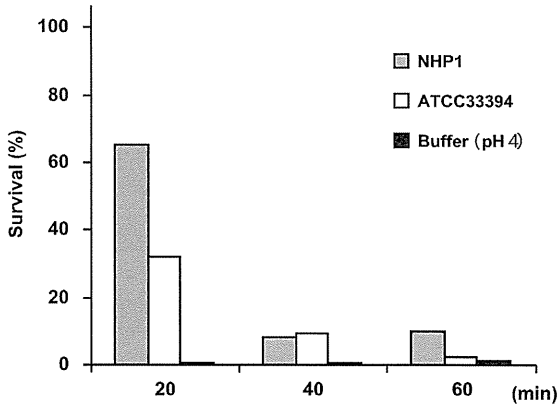

Fig. 5. Acid tolerance of *H. pylori*. Acid tolerance of *H. pylori* at 20, 40, and 60 min in the pH 4 buffer was assayed by mixing *H. pylori* CPY3401 with *K. denitrificans* NHP1, *K. denitrificans* ATCC3394, and buffer alone. Percent survival of *H. pylori* CPY3401 at pH 4 condition in contrast to pH 7 condition was calculated by comparing the numbers of colonies.

inflammation and tumorigenicity in patients with *H. pylori* infection. Conclusively, a careful administration of anti-acids to the elderly, especially those with atrophic gastritis, is required to maintain the gastric barrier to other bacteria.

Conflict of interest

The authors declare no financial or commercial conflict of interest.

Acknowledgments

The authors are grateful to M. Kimoto for providing the electronmicrograph. This work was funded partly by a Grant for Joint Research Program of the Institute for Genetic Medicine, Hokkaido University (to H.Y.) and partly by a Grant-in-Aid for Scientific Research from the Ministry of Education, Culture, Science and Technology of Japan (no. 2500163603 to Y.H.).

References

[1] Polk DB, Peek Jr RM. Helicobacter pylori: gastric cancer and beyond. Nat Rev Cancer 2010;10:403–14.
[2] Uemura N, Okamoto S, Yamamoto S, Matsumura N, Yamaguchi S, Yamakido M, et al. *Helicobacter pylori* infection and the development of gastric cancer. N Engl J Med 2001;345:784–9.
[3] Wotherspoon AC. Gastric lymphoma of mucosa-associated lymphoid tissue and *Helicobacter pylori*. Annu Rev Med 1998;49:289–99.
[4] Piccolomini R, Bonaventura GD, Festi D, Catamo G, Laterza F, Neri M. Optimal combination of media for primary isolation of *Helicobacter pylori* from gastric biopsy specimens. J Clin Microbiol. 1997;35:1541–4.
[5] Tennant SM, Hartland EL, Phumoonna T, Lyras D, Rood JI, Robins-Browne RM, et al. Influence of gastric acid on susceptibility to infection with ingested bacterial pathogens. Infect Immun 2008;76:639–45.
[6] Yoshiyama H, Nakamura H, Kimoto M, Okita K, Nakazawa T. Chemotaxis and motility of *Helicobacter pylori* in a viscous environment. J Gastroenterol 1999;34(Suppl. 11):18–23.
[7] Mine T, Muraoka H, Saika T, Kobayashi I. Characteristics of a clinical isolate of urease-negative *Helicobacter pylori* and its ability to induce gastric ulcers in Mongolian gerbils. Helicobacter 2005;10:125–31.
[8] Sahai P, West AP, Birkenhead D, Hawkey PM. *Campylobacter jejuni* in the stomach. J Med Microbiol 1995;43:75–7.
[9] Husebye E, Skar V, Hoverstad T, Melby K. Fasting hypochlorhydria with Gram positive gastric flora is highly prevalent in healthy old people. Gut 1992;33:1331–7.
[10] Sharma BK, Santana IA, Wood EC, Walt RP, Pereira M, Noone P, et al. Intragastric bacterial activity and nitrosation before, during, and after treatment with omeprazole. Br Med J 1984;289:717–9.
[11] Spiegel BM, Chey WD, Chang L. Bacterial overgrowth and irritable bowel syndrome: unifying hypothesis or a spurious consequence of proton pump inhibitors? Am J Gastroenterol 2008;103:2972–6.
[12] Nell S, Suerbaum S, Josenhans C. The impact of the microbiota on the pathogenesis of IBD: lessons from mouse infection models. Nat Rev Microbiol. 2010;8:564–77.
[13] Hassan IJ, Hayek L. Endocarditis caused by *Kingella denitrificans*. J Infect 1993;27:291–5.
[14] Rajanna DM, Manickavasagam J, Jewes L, Capper R. Retropharyngeal abscess from an unusual organism-*Kingella denitrificans*-in a patient on low-dose methotrexate. Ear Nose Throat J 2011;90:E15–7.
[15] Minamoto GY, Sordillo EM. *Kingella denitrificans* as a cause of granulomatous disease in a patient with AIDS. Clin Infect Dis 1992;15:1052–3.
[16] Zbinden R, Graevenitz AV. Actinobacillus, Capnocytophaga, Eikenella, Kingella, Pasteurella, and other fastidious or rarely encountered gram-negative rods. In: Versalovic G, Carroll KC, Funke G, Jorgensen JH, Landry ML, Warnock DW, editors. Manual of clinical microbiology. 10th ed. Washington, DC: American Society for Microbiology; 2011. pp. 582–3.
[17] Dewhirst FE, Chen CK, Paster BJ, Zambon JJ. Phylogeny of species in the family *Neisseriaceae* isolated from human dental plaque and description of *Kingella oralis* sp. nov. Int J Syst Bacteriol 1993;43:490–9.
[18] Nakamura H, Yoshiyama H, Takeuchi H, Mizote T, Okita K, Nakazawa T. Urease plays an important role in the chemotactic motility of *Helicobacter pylori* in a viscous environment. Infect Immun 1998;66:4832–7.
[19] Edwards U, Rogall T, Blocker H, Emde M, Bottger EC. Isolation and direct complete nucleotide determination of entire genes. Characterization of a gene coding for 16S ribosomal RNA. Nucleic Acid Res 1989;17:7843–53.
[20] Thompson JD, Higgins DG, Gibson TJ. CLUSTAL W: improving the sensitivity of progressive multiple sequence alignment through sequence weighting, position-specific gap penalties and weight matrix choice. Nucleic Acids Res 1994;22:4673–80.
[21] Saitou N, Nei M. The neighbour-joining method: a new method for reconstructing phylogenetic trees. Mol Biol Evol 1987;4:406–25.
[22] Pérez-Pérez GI, Olivares AZ, Cover TL, Blaser MJ. Characteristics of *Helicobacter pylori* variants selected for urease deficiency. Infect Immun 1992;60:3658–63.
[23] Rao A, Jump RL, Pultz NJ, Pultz MJ, Donskey CJ. *In vitro* killing of nosocomial pathogens by acid and acidified nitrite. Antimicrob Agents Chemother 2006;50:3901–4.
[24] Snepar R, Poporad GA, Romano JM, Kobasa WD, Kaye D. Effect of cimetidine and antacid on gastric microbial flora. Infect Immun 1982;36:518–24.
[25] Belitsos PC, Greenson JK, Yardley JH, Sisler JR, Bartlett JG. Association of gastric hypoacidity with opportunistic enteric infections in patients with AIDS. J Infect Dis 1992;166:277–84.
[26] Pettit RK, Mcallister SC, Hamer TA. Response of gonococcal clinical isolates to acidic conditions. J Med Microbiol 1999;48:149–56.
[27] Yagupsky P. *Kingella kingae*: from medical rarity to an emerging paediatric pathogen. Lancet Infect Dis 2004;4:358–67.
[28] Fostil H, Ruckdeschel G, Lang M, Eder W. Septicemia caused by *Kingella kingae*. Eur J Clin Microbiol 1984;3:267–9.
[29] Honda K, Littman DR. The microbiome in infectious disease and inflammation. Annu Rev Immunol 2012;30:759–95.
[30] Wu S, Rhee KJ, Albesiano E, Rabizadeh S, Wu X, Yen HR, et al. A human colonic commensal promotes colon tumorigenesis via activation of T helper type 17 T cell responses. Nat Med 2009;15:1016–22.
[31] Arthur JC, Perez-Chanona E, Mühlbauer M, Tomkovich S, Uronis JM, Fan TJ, et al. Intestinal inflammation targets cancer-inducing activity of the microbiota. Science 2012;338:120–3.
[32] Grivennikiv SI, Greten FR, Karin M. Immunity, inflammation, and cancer. Cell 2010;140:883–99.
[33] Kaiser P, Hardt WD. *Salmonella typhimurium* diarrhea: switching the mucosal epithelium from homeostasis to defense. Curr Opin Immunol 2011;23:456–63.

Basic Fibroblast Growth Factor Is Essential to Maintain Endothelial Progenitor Cell Phenotype in TR-BME2 Cells

Yoshimichi Sai,[a,b] Tomohiro Nishimura,[a] Mariko Muta,[a,c] Hisashi Iizasa,[a,d] Takashi Miyata,[a] and Emi Nakashima*,[a]

[a] *Division of Pharmaceutics, Faculty of Pharmacy, Keio University; 1–5–30 Shibakoen, Minato-ku, Tokyo 105–8512, Japan:* [b] *Department of Pharmacy, Kanazawa University Hospital; 13–1 Takara-machi, Kanazawa 920–8641, Japan:* [c] *Department of Health and Dietetics, Faculty of Medical Health, Teikyo Heisei University; 2–51–4 Higashi Ikebukuro, Toshima-ku, Tokyo 170–8445, Japan: and* [d] *Division of Stem Cell Biology, Institute for Genetic Medicine, Hokkaido University; Kita-15, Nishi-7, Kita-ku, Sapporo 060–0815, Japan.*

Received October 24, 2013; accepted January 19, 2014

Endothelial progenitor cells (EPC) can differentiate into both endothelial cells and contractile smooth muscle cells (SMC). Previously we reported that TR-BME2 cells, a model for EPC, developed contractile SMC-like characteristics in culture medium deprived of endothelial cell growth factors (ECGF). The aim of the present study was to clarify the effect of one of these factors, basic fibroblast growth factor (bFGF) on differentiation of EPC. First it was confirmed that bFGF receptor (FGFR-1) mRNA is expressed in TR-BME2 cultured in both ECGF-rich and ECGF-deprived medium. When TR-BME2 cells were cultured in ECGF-deprived medium, they differentiated into contractile SMC. Expression of an undifferentiated state marker, CD133, and proliferation of TR-BME2 were both reduced by ECGF deprivation, but these changes were diminished in the presence of bFGF. mRNA expression of smooth muscle α-actin (SMA) and smooth muscle protein 22 (SM22), which are contractile SMC markers, was induced by deprivation of ECGF and the induction was suppressed by bFGF. In vascular endothelial cell growth factor (VEGF)-induced tube formation assay, TR-BME2 cells formed tube structures in the presence of bFGF, but not in its absence. Our results indicate that bFGF is essential for the maintenance of EPC phenotype, serving to suppress differentiation to contractile SMC.

Key words endothelial progenitor cell; vasculogenesis; differentiation; vascular smooth muscle cell; proliferation; tube formation

Endothelial progenitor cells (EPC) are derived from bone marrow and differentiation of EPC to endothelial cells (EC) and smooth muscle cells (SMC) contributes to vasculogenesis in adults.[1,2] Both EC and mural cells, consisting of SMC and pericytes, contribute to the development and maintenance of the vasculature. The contribution of EPC to vasculogenesis in adults was reported to be around 10%.[3] However, the factors controlling differentiation of EPC to EC or SMC remain unclear. Differentiation of stem cells and progenitor cells is regulated by cytokines such as basic fibroblast growth factor (bFGF also known as FGF2). For instance, neural stem cells are maintained in the undifferentiated state by bFGF, and begin to differentiate to neuronal cells or astrocytes if deprived of bFGF.[4] bFGF is also involved in survival of angioblasts, which play a role in vasculogenesis.[5] However, it is not clear whether bFGF acts to maintain the undifferentiation state of EPC.

EPC characteristically express CD133, CD34, and Flk-1 (also known as vascular endothelial growth factor receptor-2 (VEGFR-2)), while mature EC express CD34 and Flk-1.[6,7] EPC loses CD133 expression in the systemic circulation, so that CD133 is a marker for early EPC.[8,9] CD133, CD34 and Flk-1-positive EPC show chemotactic activity in the presence of vascular endothelial cell growth factor (VEGF).[8,10,11] For further study, we have established a conditionally immortalized bone marrow-derived EPC line clone 2, namely TR-BME2, derived from temperature-sensitive SV40 transgenic rats.[12] TR-BME2 cells express CD133, CD34, Flk-1 von Willebrand factor and annexin II.[2,12] Fluorescence-labeled TR-BME2 cells injected systemically into tumor-bearing rats accumulated into the solid tumors, induced vasculogenesis and promoted tumor growth, suggesting that TR-BME2 cells have potential to differentiate into EC in response to VEGF.[13–15] TR-BME2 cells are cultured in endothelial cell growth medium-2 (EGM-2) medium, which contains several endothelial cell growth factors (ECGF) that are required to maintain the characteristics of EPC.

SMC have two phenotypes, *i.e.*, contractile and synthetic.[16] Contractile SMC express smooth muscle α-actin (SMA) and smooth muscle protein 22 (SM22) as markers, and have the ability to contract in response to vasoconstricting messages.[17,18] We have shown that TR-BME2 cells differentiate to contractile SMC on culture in ECGF-deprived endothelial cell basal medium-2 (EBM-2) medium, and the contractile SMC further differentiate to synthetic SMC in the presence of platelet-derived growth factor (PDGF)-BB.[2] Therefore, TR-BME2 cells have the potential to differentiate into either EC or SMC. It is possible that some factor(s) in ECGF is involved in maintaining the undifferentiated state of EPC, but so far it has not identified. EGM-2 medium contains bFGF, VEGF, epidermal growth factor (EGF) and insulin-like growth factor (IGF) as ECGF. We hypothesized that bFGF is involved in suppression of differentiation of EPC to contractile SMC. Therefore, the aim of this study was to test this idea by examining the effect of bFGF on differentiation of EPC. We used TR-BME2 cells as a model for EPC.

The authors declare no conflict of interest.

* To whom correspondence should be addressed. e-mail: nakashima-em@pha.keio.ac.jp

MATERIALS AND METHODS

Cell Culture Rat bone marrow EPC-derived cell line clone 2, TR-BME2, was used as described below.[12] TR-BME2 cells were maintained on human plasma fibronectin (Life Technologies Inc., Rockville, MD, U.S.A.) and type I collagen-coated dishes (Iwaki, Tokyo, Japan) in EGM-2 medium, *i.e.*, Endothelial Basal Medium-2 (EBM-2; Clontech, San Diego, CA, U.S.A.) supplemented with EGM-2 BulletKit (Clontech Laboratories, Mountain View, CA, U.S.A.) (except for hydrocortisone), bFGF, VEGF, EGF, IGF-1, ascorbic acid, heparin, gentamicin and fetal bovine serum (FBS). To investigate the effect of each growth factor, the EBM-2 was supplemented with that given growth factor, *i.e.*, human bFGF (Sigma-Aldrich, St. Louis, MO, U.S.A.), human VEGF (Strathmann Biotec GmbH & Co., KG, Hamburg, Germany), EGF (bundled in the EGM-2 BulletKit) or IGF (bundled in the EGM-2 BulletKit), together with other components mentioned above. Cells were incubated at 37°C in a humidified 5% CO_2 incubator.

Reverse Transcription-Polymerase Chain Reaction (RT-PCR) Analysis mRNA expression of rat glyceraldehyde-3-phosphate dehydrogenase (G3PDH), rat FGF receptor-1 (FGFR-1) and rat CD133 in TR-BME2 was analyzed by RT-PCR analysis. DNA sequences of the sense and anti-sense primers are shown in Table 1. Total RNA was isolated by the acid phenol procedure using ISOGEN reagent (Wako Pure Chemical Industries, Ltd., Tokyo, Japan) according to the manufacturer's protocol. RT was performed from 1 μg of total RNA using oligo $(dT)_{15}$ as a primer and M-MLV reverse transcriptase (ReverTraAce; Toyobo Co., Ltd., Osaka, Japan). RT-PCR was conducted using Platinum PCR SuperMix (Life Technologies Inc.). The reaction was carried out for 18 to 35 cycles of 94°C, 15 s for denaturing; 58 or 68°C, 20 s for annealing; and 72°C, 1 min for extension. PCR products were visualized by ethidium bromide staining after resolution on 5% acrylamide gel. They were subcloned into a plasmid vector using pGEM-T Easy Vector System I (Promega, Madison, WI, U.S.A.) and then sequenced from both directions using a DNA sequencer (CEQ2000XL DNA Analysis System; Beckman Coulter, Fullerton, CA, U.S.A.). The sequences of PCR products were confirmed to be consistent with the corresponding reference sequence.

Cell Proliferation Assay TR-BME2 cells were cultured on 96-well plate in EGM-2 or EBM-2 medium in the absence or presence of bFGF at 37°C for 72 h. Cell number was as-

Table 1. Primers Used for RT-PCR Analysis

	Sense primer (5′–3′)	Anti-sense primer (5′–3′)
G3PDH	GCATGGCCTTCCGTGTTCCTA	GTCCACCACCACCCTGTTGCTGT
FGFR-1	GCGTGCCTGTGGAAGAAC	ACTCCTGGTTGGAGGTCAAG
CD133	AAGCAGCAAGTTGCCGGAGGAA	GTCATCTTCTCTGTGATGGCGTACA
SMA	GCTATGCTCTGCCTCATG	TTCATTCCCGATGGTGATCA
SM22	GCAGCAGTGCAGAGGACTGTA	GGTCGCCCATAGCCTGTCA

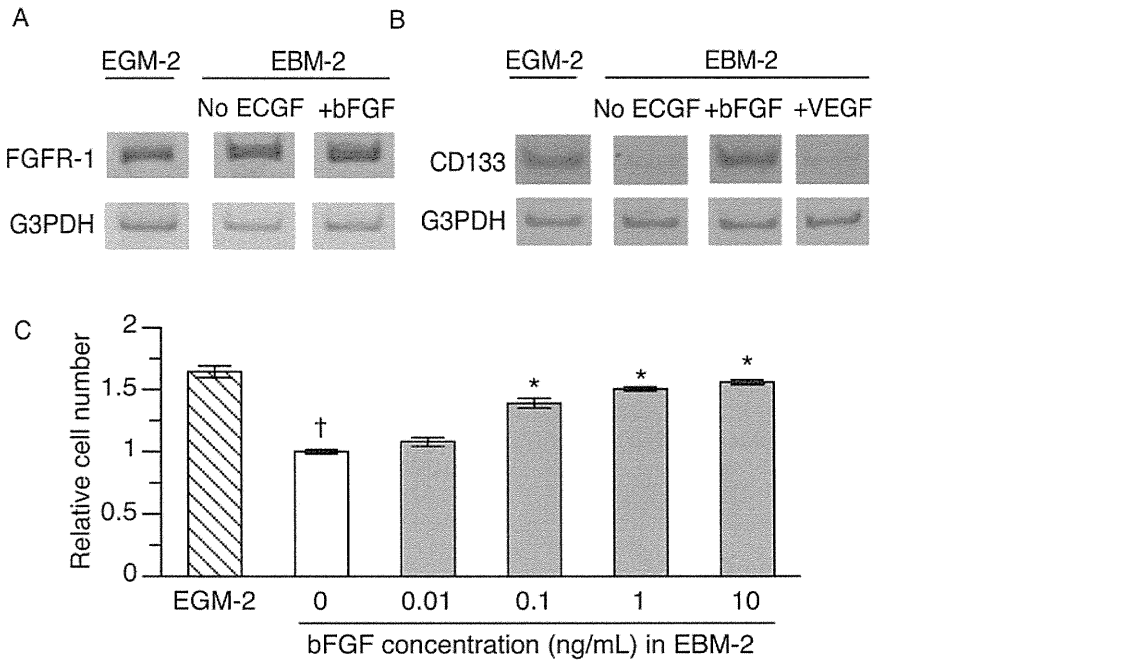

Fig. 1. Effects of bFGF on Maintenance of the Undifferentiated State and on Proliferation of TR-BME2 Cells

mRNA expression of FGFR-1 (A), CD133 (B) and G3PDH in TR-BME2 cells cultured by EGM-2 (hatched column) or EBM-2 medium in the presence (closed column) and absence (open column) of 20 ng/mL bFGF or 25 ng/mL VEGF at 37°C for 8 d were analyzed by RT-PCR. The PCR products were electrophoresed on 5% acrylamide gel and then visualized by ethidium bromide staining. (C) TR-BME2 cells were cultured in EGM-2, or EBM-2 medium in the presence of bFGF in the concentration range of 0–10 ng/mL at 37°C for 72 h. Cell number was assessed by WST-1 assay. Each column represents the mean±S.E.M. (n=3). Statistical significance of differences was analyzed by Student's t-test between EGM-2 (hatched column) and the no-ECGF control (white column) as shown by (†) and by ANOVA with Dunnett's multiple comparison test compared to the no-ECGF control (open column) as shown by (*). A p value of less than 0.05 was regarded as significant.

sessed by measuring mitochondrial reduced nicotinamide adenine dinucleotide (NADH)-dependent dehydrogenase activity using Cell Counting Kit (Dojindo Laboratories, Kumamoto, Japan) containing WST-1. Cells were added with 10 μL of 5 μg/mL WST-1 and incubated for 1 h at 37°C in 5% CO_2 incubator. Then, absorbance at 450 nm was measured.

Quantitative Real-Time PCR Analysis (qPCR) qPCR analysis was performed using an ABI PRISM 7700 sequence detector system (PE Applied Biosystems, Foster City, CA, U.S.A.) with 2× SYBR Green PCR Master Mix (Life Technologies Inc.) as per the manufacturer's protocol. To quantify the amount of specific mRNA in the samples, a standard curve was generated for each run using pGEM-T Easy Vector. Relative expression of a specific gene compared to G3PDH expression was also quantified. The control lacking the RT enzyme was assayed in parallel to check for genomic contamination. PCR was performed through 40 cycles of 95°C for 30 s, 60°C for 1 min, and 72°C for 1 min after pre-incubation at 95°C for 10 min using specific primers.

Tube Formation Assay TR-BME2 cells were precultured in EGM-2 or EBM-2 medium in the absence or presence of bFGF (20 ng/mL) or VEGF (25 ng/mL) for 8 d. Matrigel (Becton Dickinson, Bedford, MA, U.S.A.) was used to coat a 24-well culture plate (0.25 mL/well). After polymerization of the Matrigel at 37°C for 1 h, cells suspended in 0.5 mL of EBM-2 supplemented with 25 ng/mL VEGF (4×10^4 cells/well) were transferred to the gel and incubated at 37°C for 5 h. Tube formation of the cells were observed using a conventional bright-field microscope. Numbers of the tube like structures were counted in randomly selected fields.

Statistical Analysis Data are presented as a percentage of the value for untreated control culture and shown as mean± S.E.M. (n=3). The significance of differences was evaluated by means of one-way ANOVA with Dunnett's multiple comparison test. The criterion of significance was a p value less than 0.05.

RESULTS

FGFR-1 Expression in TR-BME2 Cells EGM-2 medium is composed of EBM-2 medium with several ECGF supplements. To analyze the effect of bFGF and other growth factors included in EGM-2 medium, we used EBM-2 medium supplemented with a single designated growth factor and the other additives. First, we measured the expression of rat fibroblast growth factor receptor (FGFR-1) in TR-BME2 cells cultured in ECGF-deprived EBM-2 medium and in EGM-2. FGFR-1 mRNA was expressed in TR-BME2 cells in both media, and exposure of TR-BME2 to bFGF did not change the expression level of FGFR-1 (Fig. 1A).

Effect of bFGF on Undifferentiated State and Proliferation of TR-BME2 Cells To investigate whether bFGF contributes to maintenance of the undifferentiated state and proliferation of TR-BME2 cells, we measured mRNA expression of CD133 and viability in the presence of bFGF. TR-BME2 cells cultured in ECGF-deprived EBM-2 medium showed a reduction of CD133 expression. The expression of CD133 was maintained in EBM-2 medium supplemented with bFGF, whereas VEGF was ineffective (Fig. 1B). The proliferation rate of TR-BME2 cells cultured in EBM-2 medium was increased approximately 1.5-fold by the addition of bFGF in a concentration-dependent manner (Fig. 1C), and was similar to that of cells cultured in EGM-2 medium.

Effect of bFGF on a Contractile SMC Marker To clarify the effect of bFGF on expression of a contractile SMC marker, SMA, we measured mRNA expression of SMA in the presence of various growth factors. Although VEGF, EGF and IGF did not change the expression of SMA in TR-BME2 cells cultured in EBM-2 medium compared to the no-ECGF control, SMA expression in cells cultured in the presence of bFGF was

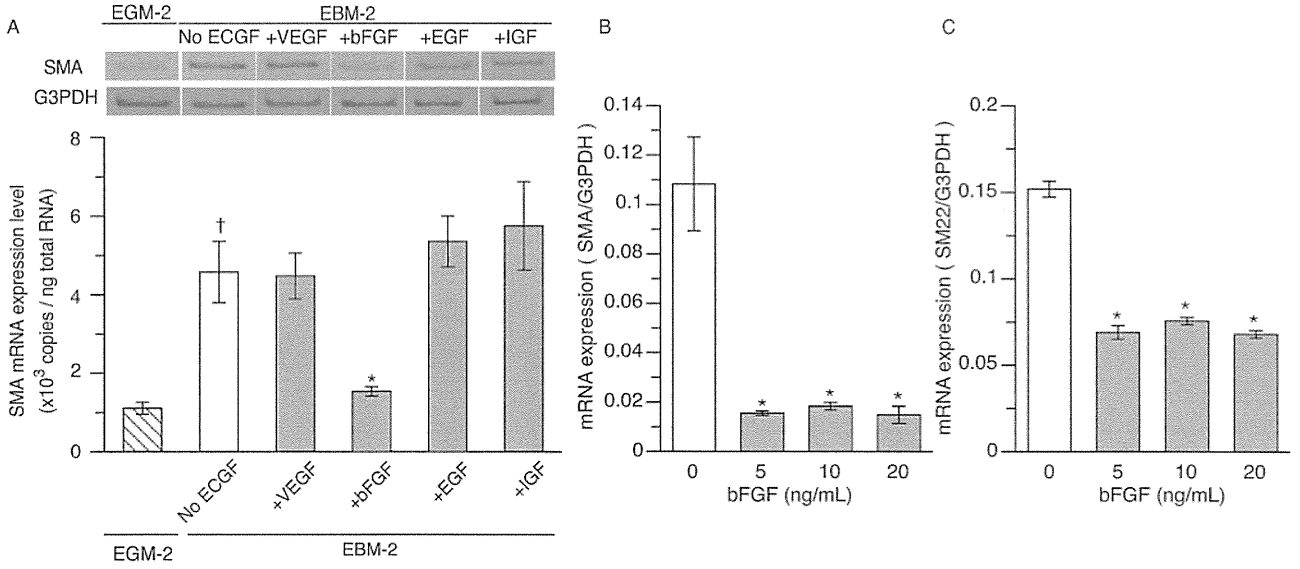

Fig. 2. Effect of bFGF on Differentiation of TR-BME2 Cells

Quantitative RT-PCR for vascular smooth muscle cell markers, SMA and SM22, was performed. (A) TR-BME2 cells were cultured in EGM-2 (hatched column), or EBM-2 medium in the presence (closed column) and absence (open column) of 20 ng/mL bFGF, 25 ng/mL VEGF, EGF or IGF at 37°C for 10 d. Representative PCR products of SMA and G3PDH as a loading control were electrophoresed (upper panel) and the mRNA copy number per ng total RNA was determined (lower panel). (B, C) TR-BME2 cells were cultured in EBM-2 medium in the presence (closed column) and absence (open column) of bFGF at 37°C for 10 d. Relative mRNA expression of SMA and SM22 normalized by G3PDH was shown in panels B and C, respectively. Statistical significance was analyzed by Student's t-test between EGM-2 (hatched column) and the no-ECGF control (white column) as shown by (†) and by ANOVA with Dunnett's multiple comparison test compared to the no-ECGF control (open column) as shown by (*). A p value of less than 0.05 was regarded as significant.

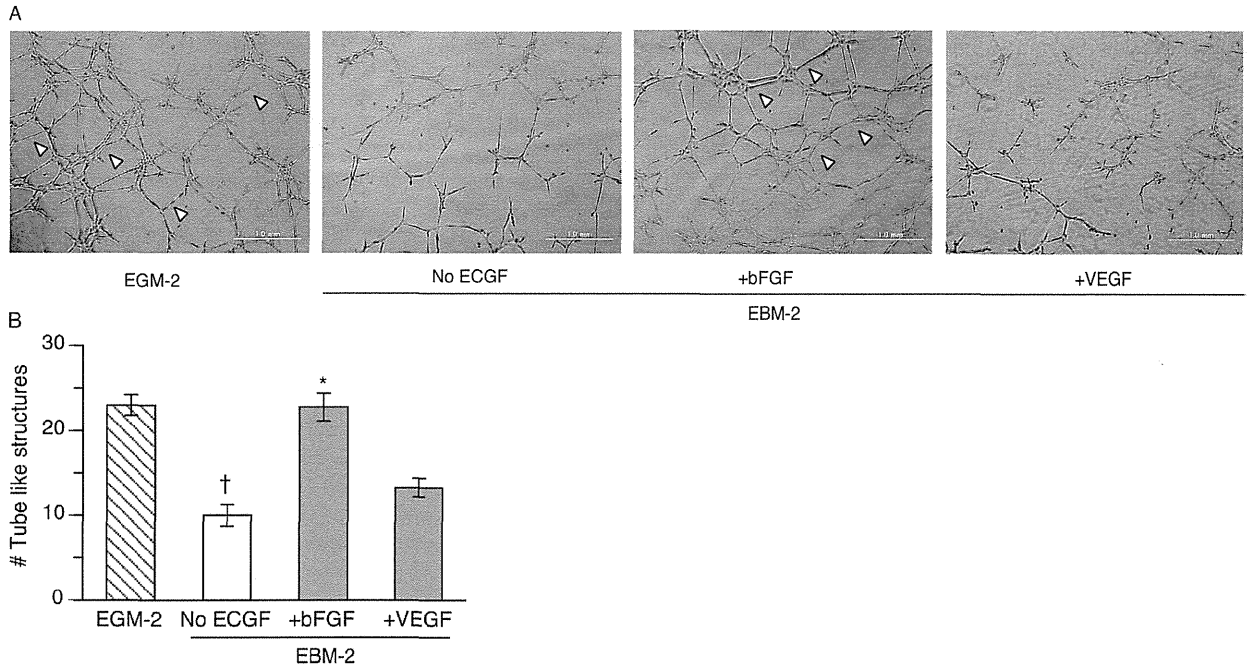

Fig. 3. Tube Formation of TR-BME2 on Matrigel

TR-BME2 cells were cultured in EGM-2, or EBM-2 medium in the presence or absence of 20 ng/mL bFGF or 25 ng/mL VEGF for 8 d. (A) Tube formation of the cells on Matrigel-coated well was analyzed by bright-field images as described in Materials and Methods. Arrowheads indicate representative tube structure. (B) Numbers of the tube like structures were counted as described in Materials and Methods. Statistical significance of differences was analyzed by Student's *t*-test between EGM-2 (hatched column) and the no-ECGF control (white column) as shown by (†) and by ANOVA with Dunnett's multiple comparison test compared to the no-ECGF control (open column) as shown by (*). A p value of less than 0.05 was regarded as significant.

significantly lower, being similar to that of cells cultured in EGM-2 medium (Fig. 2A). SMA mRNA expression and SM22 mRNA expression normalized by G3PDH were more than 5-fold and 2-fold suppressed, respectively, by the addition of bFGF in the concentration range of 5–20 ng/mL (Figs. 2B, C).

Effect of bFGF on Tube Formation from EPC To address the effect of bFGF on the differentiation potential of EPC to EC, tube formation by VEGF-exposed cells was examined. TR-BME2 cells precultured in EGM-2 medium formed tubes (Fig. 3A). TR-BME2 cells precultured in EBM-2 medium in the presence or absence of VEGF alone little formed tubes, but they did form tubes if they had been pretreated with bFGF (Fig. 3A). Counting of tube-like structures indicate a significant increase of tube structure by bFGF treatment, which is almost equal to the number pretreated in EGM-2 medium (Fig. 3B).

DISCUSSION

TR-BME2 cells are cultured in EGM-2 medium containing ECGF to maintain the characteristics of EPC. TR-BME2 cells cultured in EGM-2 showed expression of CD133 (Fig. 1B) and little expression of SMA (Fig. 2A). However, TR-BME2 cells cultured in ECGF-deprived EBM-2 showed down-regulation of CD133 and up-regulation of SMA (Figs. 1B, 2A). Therefore, TR-BME2 cultured in EGM-2 medium and in ECGF-deprived EBM-2 medium exhibit EPC-like and SMC-like phenotype, respectively. These results confirmed the ability of TR-BME2 to undergo EPC-like differentiation to SMC, as we have reported.[2] Among the ECGF, we found that bFGF increased viability and CD133 expression (Fig. 1). These results are consistent with reports that human umbilical vein endothelial cell (HUVEC) migrate in response to bFGF.[19] EPC express FGFR-1, and two isoforms of FGFR-1 generated by alternative splicing, *i.e.*, FGFR-1b and FGFR-1c, accept bFGF as a ligand.[20,21] Both EPC-like and SMC-like TR-BME2 showed expression of FGFR-1 (Fig. 1). The effect of ECGF on FGFR-1 expression was minimal (Fig. 1). TR-BME2 cultured in ECGF-deprived medium showed induction of SMA, and addition of bFGF alone suppressed SMA induction (Fig. 2). The suppression of SMA mRNA expression by bFGF was saturated at 5 ng/mL and further suppression was not observed (Fig. 2). The suppression of differentiation from EPC to SMC was also associated with suppression of SM22, but the effect of bFGF on SM22 was smaller than that in the case of SMA (Fig. 2). These findings indicate that bFGF plays a role in maintenance of the undifferentiated state of EPC.

TR-BME2 cells have the ability to differentiate to EC and form tube structure on culture in EGM-2 medium (Fig. 3), like human EPC.[22] Addition of VEGF to TR-BME2 cells cultured in ECGF-deprived medium did not induce CD133 expression, influence SMA expression, or induce tube formation (Figs. 1B, 2A, 3), implying that TR-BME2 cells cultured in ECGF-deprived medium remain as SMC. Supplementation of bFGF enabled VEGF-induced tube formation of TR-BME2 cells (Fig. 3). bFGF is also involved in tube formation of adipose-tissue-derived stem cells.[23] bFGF and PDGF-BB synergistically release VEGF from EPC and promote tumor neovascularization.[24,25] These results indicate that EPC require bFGF for maintenance of tube-forming potential.

bFGF enhances proliferation of retinal vascular endothelial cells by activating extracellular signal-regulated kinase (ERK)1/2 and Akt.[26] ERK1/2 and migration of EC are less activated in bFGF knockout mice compared to wild-type mice.[27] bFGF activates ERK in SMC, and the cells are dedifferentiated, promoting proliferation.[28] Taken together, the

above findings suggest that bFGF plays a role in maintenance of undifferentiation and proliferation in EPC *via* ERK and Akt signaling pathways before activation by VEGF for vasculogenesis.

Therapeutic vasculogenesis is useful for rescue of peripheral and circulatory organs from ischemia.[29,30] VEGF-transduced EPC transplantation required 30 times fewer cells than cell therapy alone, and contributed to *in vivo* neovascularization.[29] Therefore, EPC are useful for therapeutic vasculogenesis. But, to effectively utilize bone-marrow derived EPC for therapy, it is important to control differentiation of EPC to EC or SMC.

In conclusion, bFGF has roles in maintenance of the undifferentiated state and in proliferation of EPC, allowing EPC to maintain the potential to differentiate to EC. Lack of bFGF exposure leads EPC to differentiate to contractile SMC. Thus, controlled exposure of EPC to bFGF could be useful for therapeutic vasculogenesis.

Acknowledgments This study was supported in part by a Grant-in-Aid for Scientific Research from Japan Society for the Promotion of Science (JSPS), and from the MEXT-Supported Program for the Strategic Research Foundation at Private Universities.

REFERENCES

1) Asahara T, Murohara T, Sullivan A, Silver M, van der Zee R, Li T, Witzenbichler B, Schatteman G, Isner JM. Isolation of putative progenitor endothelial cells for angiogenesis. *Science*, **275**, 964–967 (1997).
2) Miyata T, Iizasa H, Sai Y, Fujii J, Terasaki T, Nakashima E. Platelet-derived growth factor-BB (PDGF-BB) induces differentiation of bone marrow endothelial progenitor cell-derived cell line TR-BME2 into mural cells, and changes the phenotype. *J. Cell. Physiol.*, **204**, 948–955 (2005).
3) Crosby JR, Kaminski WE, Schatteman G, Martin PJ, Raines EW, Seifert RA, Bowen-Pope DF. Endothelial cells of hematopoietic origin make a significant contribution to adult blood vessel formation. *Circ. Res.*, **87**, 728–730 (2000).
4) Enarsson M, Erlandsson A, Larsson H, Forsberg-Nilsson K. Extracellular signal-regulated protein kinase signaling is uncoupled from initial differentiation of central nervous system stem cells to neurons. *Mol. Cancer Res.*, **1**, 147–154 (2002).
5) Kazemi S, Wenzel D, Kolossov E, Lenka N, Raible A, Sasse P, Hescheler J, Addicks K, Fleischmann BK, Bloch W. Differential role of bFGF and VEGF for vasculogenesis. *Cell. Physiol. Biochem.*, **12**, 55–62 (2002).
6) Gehling UM, Ergun S, Schumacher U, Wagener C, Pantel K, Otte M, Schuch G, Schafhausen P, Mende T, Kilic N, Kluge K, Schafer B, Hossfeld DK, Fiedler W. *In vitro* differentiation of endothelial cells from AC133-positive progenitor cells. *Blood*, **95**, 3106–3112 (2000).
7) Shalaby F, Ho J, Stanford WL, Fischer KD, Schuh AC, Schwartz L, Bernstein A, Rossant J. A requirement for Flk1 in primitive and definitive hematopoiesis and vasculogenesis. *Cell*, **89**, 981–990 (1997).
8) Hristov M, Erl W, Weber PC. Endothelial progenitor cells: mobilization, differentiation, and homing. *Arterioscler. Thromb. Vasc. Biol.*, **23**, 1185–1189 (2003).
9) Yin AH, Miraglia S, Zanjani ED, Almeida-Porada G, Ogawa M, Leary AG, Olweus J, Kearney J, Buck DW. AC133, a novel marker for human hematopoietic stem and progenitor cells. *Blood*, **90**, 5002–5012 (1997).
10) Asahara T, Masuda H, Takahashi T, Kalka C, Pastore C, Silver M, Kearne M, Magner M, Isner JM. Bone marrow origin of endothelial progenitor cells responsible for postnatal vasculogenesis in physiological and pathological neovascularization. *Circ. Res.*, **85**, 221–228 (1999).
11) Peichev M, Naiyer AJ, Pereira D, Zhu Z, Lane WJ, Williams M, Oz MC, Hicklin DJ, Witte L, Moore MA, Rafii S. Expression of VEGFR-2 and AC133 by circulating human CD34(+) cells identifies a population of functional endothelial precursors. *Blood*, **95**, 952–958 (2000).
12) Hattori K, Muta M, Toi M, Iizasa H, Shinsei M, Terasaki T, Obinata M, Ueda M, Nakashima E. Establishment of bone marrow-derived endothelial cell lines from ts-SV40 T-antigen gene transgenic rats. *Pharm. Res.*, **18**, 9–15 (2001).
13) Muta M, Matsumoto G, Hiruma K, Nakashima E, Toi M. Study of cancer gene therapy using IL-12-secreting endothelial progenitor cells in a rat solid tumor model. *Oncol. Rep.*, **10**, 1765–1769 (2003).
14) Muta M, Matsumoto G, Hiruma K, Saji S, Nakashima E, Toi M. Impact of vasculogenesis on solid tumor growth in a rat model. *Oncol. Rep.*, **10**, 1213–1218 (2003).
15) Muta M, Yanagawa T, Sai Y, Saji S, Suzuki E, Aruga T, Kuroi K, Matsumoto G, Toi M, Nakashima E. Effect of low-dose paclitaxel and docetaxel on endothelial progenitor cells. *Oncology*, **77**, 182–191 (2009).
16) Iehara N, Takeoka H, Tsuji H, Imabayashi T, Foster DN, Strauch AR, Yamada Y, Kita T, Doi T. Differentiation of smooth muscle phenotypes in mouse mesangial cells. *Kidney Int.*, **49**, 1330–1341 (1996).
17) Adam PJ, Regan CP, Hautmann MB, Owens GK. Positive- and negative-acting Kruppel-like transcription factors bind a transforming growth factor beta control element required for expression of the smooth muscle cell differentiation marker SM22alpha *in vivo*. *J. Biol. Chem.*, **275**, 37798–37806 (2000).
18) Hu WY, Fukuda N, Satoh C, Jian T, Kubo A, Nakayama M, Kishioka H, Kanmatsuse K. Phenotypic modulation by fibronectin enhances the angiotensin II-generating system in cultured vascular smooth muscle cells. *Arterioscler. Thromb. Vasc. Biol.*, **20**, 1500–1505 (2000).
19) Yoshida A, Anand-Apte B, Zetter BR. Differential endothelial migration and proliferation to basic fibroblast growth factor and vascular endothelial growth factor. *Growth Factors*, **13**, 57–64 (1996).
20) Burger PE, Coetzee S, McKeehan WL, Kan M, Cook P, Fan Y, Suda T, Hebbel RP, Novitzky N, Muller WA, Wilson EL. Fibroblast growth factor receptor-1 is expressed by endothelial progenitor cells. *Blood*, **100**, 3527–3535 (2002).
21) Eswarakumar VP, Lax I, Schlessinger J. Cellular signaling by fibroblast growth factor receptors. *Cytokine Growth Factor Rev.*, **16**, 139–149 (2005).
22) Bagley RG, Walter-Yohrling J, Cao X, Weber W, Simons B, Cook BP, Chartrand SD, Wang C, Madden SL, Teicher BA. Endothelial precursor cells as a model of tumor endothelium: characterization and comparison with mature endothelial cells. *Cancer Res.*, **63**, 5866–5873 (2003).
23) Gehmert S, Gehmert S, Hidayat M, Sultan M, Berner A, Klein S, Zellner J, Muller M, Prantl L. Angiogenesis: the role of PDGF-BB on adipose-tissue derived stem cells (ASCs). *Clin. Hemorheol. Microcirc.*, **48**, 5–13 (2011).
24) Sufen G, Xianghong Y, Yongxia C, Qian P. bFGF and PDGF-BB have a synergistic effect on the proliferation, migration and VEGF release of endothelial progenitor cells. *Cell Biol. Int.*, **35**, 545–551 (2011).
25) Nissen LJ, Cao R, Hedlund EM, Wang Z, Zhao X, Wetterskog D, Funa K, Brakenhielm E, Cao Y. Angiogenic factors FGF2 and PDGF-BB synergistically promote murine tumor neovascularization and metastasis. *J. Clin. Invest.*, **117**, 2766–2777 (2007).
26) Zubilewicz A, Hecquet C, Jeanny JC, Soubrane G, Courtois Y, Mascarelli F. Two distinct signalling pathways are involved in FGF2-stimulated proliferation of choriocapillary endothelial cells: a

comparative study with VEGF. *Oncogene*, **20**, 1403–1413 (2001).
27) Pintucci G, Moscatelli D, Saponara F, Biernacki PR, Baumann FG, Bizekis C, Galloway AC, Basilico C, Mignatti P. Lack of ERK activation and cell migration in FGF-2-deficient endothelial cells. *FASEB J.*, **16**, 598–600 (2002).
28) Hayashi K, Takahashi M, Kimura K, Nishida W, Saga H, Sobue K. Changes in the balance of phosphoinositide 3-kinase/protein kinase B (Akt) and the mitogen-activated protein kinases (ERK/p38MAPK) determine a phenotype of visceral and vascular smooth muscle cells. *J. Cell Biol.*, **145**, 727–740 (1999).
29) Iwaguro H, Yamaguchi J, Kalka C, Murasawa S, Masuda H, Hayashi S, Silver M, Li T, Isner JM, Asahara T. Endothelial progenitor cell vascular endothelial growth factor gene transfer for vascular regeneration. *Circulation*, **105**, 732–738 (2002).
30) Atluri P, Panlilio CM, Liao GP, Hiesinger W, Harris DA, McCormick RC, Cohen JE, Jin T, Feng W, Levit RD, Dong N, Woo YJ. Acute myocardial rescue with endogenous endothelial progenitor cell therapy. *Heart Lung Circ.*, **19**, 644–654 (2010).

JVI
Journals.ASM.org

Clustered MicroRNAs of the Epstein-Barr Virus Cooperatively Downregulate an Epithelial Cell-Specific Metastasis Suppressor

Teru Kanda,[a] Mamiko Miyata,[a] Makoto Kano,[b] Satoru Kondo,[b] Tomokazu Yoshizaki,[b] Hisashi Iizasa[c]

Division of Microbiology and Oncology, Aichi Cancer Center Research Institute, Chikusa-ku, Nagoya, Japan[a]; Division of Otolaryngology-Head and Neck Surgery, Graduate School of Medical Science, Kanazawa University, Kanazawa, Ishikawa, Japan[b]; Department of Microbiology, Shimane University Faculty of Medicine, Izumo, Shimane, Japan[c]

ABSTRACT

The Epstein-Barr virus (EBV) encodes its own microRNAs (miRNAs); however, their biological roles remain elusive. The commonly used EBV B95-8 strain lacks a 12-kb genomic region, known as BamHI A rightward transcripts (BART) locus, where a number of BART miRNAs are encoded. Here, bacterial artificial chromosome (BAC) technology was used to generate an EBV B95-8 strain in which the 12-kb region was fully restored at its native locus [BART(+) virus]. Epithelial cells were stably infected with either the parental B95-8 virus or the BART(+) virus, and BART miRNA expression was successfully reconstituted in the BART(+) virus-infected cells. Microarray analyses of cellular gene expression identified N-myc downstream regulated gene 1 (*NDRG1*) as a putative target of BART miRNAs. The NDRG1 protein was barely expressed in B cells, highly expressed in epithelial cells, including primary epithelial cells, and strongly downregulated in the BART(+) virus-infected epithelial cells of various origins. Although *in vitro* reporter assays identified BART22 as being responsible for the NDRG1 downregulation, EBV genetic analyses revealed that BART22 was not solely responsible; rather, the entire BART miRNA cluster 2 was responsible for the downregulation. Immunohistochemical analyses revealed that the expression level of the NDRG1 protein was downregulated significantly in EBV-positive nasopharyngeal carcinoma specimens. Considering that *NDRG1* encodes an epithelial differentiation marker and a suppressor of metastasis, these data implicate a causative relationship between BART miRNA expression and epithelial carcinogenesis *in vivo*.

IMPORTANCE

EBV-related epithelial cancers, such as nasopharyngeal carcinomas and EBV-positive gastric cancers, encompass more than 80% of EBV-related malignancies. Although it is known that they express high levels of virally encoded BART miRNAs, how these miRNAs contribute to EBV-mediated epithelial carcinogenesis remains unknown. Although a number of screenings have been performed to identify targets of viral miRNAs, many targets likely have not been identified, especially in case of epithelial cell infection. This is the first study to use EBV genetics to perform unbiased screens of cellular genes that are differentially expressed in viral miRNA-positive and -negative epithelial cells. The result indicates that multiple EBV-encoded miRNAs cooperatively downregulate NDRG1, an epithelial differentiation marker and suppressor of metastasis. The experimental system described in this study should be useful for further clarifying the mechanism of EBV-mediated epithelial carcinogenesis.

The Epstein-Barr virus (EBV) is a common herpesvirus that is widespread in all human populations. Primary EBV infections in adolescence often manifest as infectious mononucleosis (1). EBV infection is also associated with several types of lymphomas and epithelial malignancies. The B95-8 strain of EBV, an infectious mononucleosis-derived isolate, is biologically indistinguishable from other isolates of EBV in that it efficiently produces progeny virus and transforms peripheral B-lymphocytes *in vitro* (2). The marmoset lymphoblastoid B95-8 cell line is one of the most widely used EBV-producing cell lines. Although the B95-8 strain was assumed to be a prototype EBV, restriction mapping and DNA sequencing analyses revealed that its genome contains a deletion of approximately 12 kb (3–5). This deleted region is apparently dispensable for progeny virus production and B-cell transformation; hence, its importance has been underestimated.

The recent discovery of EBV-encoded microRNA (miRNA) genes within the 12-kb region has dramatically changed the situation. The initial discovery of five EBV miRNAs was followed by the subsequent identification of a number of additional miRNAs (6–9); to date, 44 mature miRNAs have been identified, of which 4 are encoded at the *BHRF1* locus, and 40 are encoded at the BART locus. A complete list of EBV miRNAs, including their mature and precursor sequences, is available at miRBase (www.mirbase.org). BART miRNAs are of particular interest because 17 of their 22 pre-miRNAs are located within the B95-8 deleted region. When studies were conducted to identify genes that were uniquely expressed in EBV-infected epithelial cells, this region was found to be actively transcribed in nasopharyngeal carcinoma (NPC) cells (10, 11). The transcripts were named as complementary-strand

Received 5 November 2014 Accepted 11 December 2014
Accepted manuscript posted online 17 December 2014
Citation Kanda T, Miyata M, Kano M, Kondo S, Yoshizaki T, Iizasa H. 2015. Clustered microRNAs of the Epstein-Barr virus cooperatively downregulate an epithelial cell-specific metastasis suppressor. J Virol 89:2684–2697. doi:10.1128/JVI.03189-14.
Editor: R. M. Longnecker
Address correspondence to Teru Kanda, tkanda@aichi-cc.jp.
Supplemental material for this article may be found at http://dx.doi.org/10.1128/JVI.03189-14.

doi:10.1128/JVI.03189-14

transcripts (10), BARF0 (12), or BARTs (13). Whether the transcripts are translated to one or more proteins remains enigmatic; however, it is now clear that they serve as primary transcripts that are processed to generate mature BART miRNAs. BART miRNAs are derived from BART introns prior to splicing (14). Similar to the high expression levels of BART RNAs in epithelial cells, BART miRNAs are also expressed at high levels in NPC cells (9, 15) and in gastric carcinoma cells (16). BART miRNAs are also expressed at high levels in NK/T lymphoma-derived cell lines (17). On the other hand, few viral proteins are expressed in EBV-infected epithelial cells, suggesting that BART miRNAs contribute to epithelial tumorigenesis (18–20).

Many target proteins of BART miRNAs have been identified to date. Those that are encoded by EBV itself include BALF5 (21), LMP1 (22), LMP2A (23), and BHRF1 (23, 24). Previously identified cellular targets include Bim (25), CAPRIN2 (24), CASP3 (26), DAZAP2 (27), DICER1 (28), E-cadherin (29), IPO7 (26, 30), and PUMA (31). Many other candidate target genes have been identified by miRNA targetome studies (24, 27, 30, 32); the biological significances of these miRNA-target interactions have yet to be clarified. BART miRNA targets in epithelial cells have not been explored extensively; thus, many targets have probably not been identified.

The high expression levels of BART miRNAs in epithelial cells suggest that the B95-8 strain of EBV, which lacks many of the BART pre-miRNA genes, is phenotypically different from wild-type EBV. Thanks to the recent development of bacterial artificial chromosome (BAC) systems that enable the manipulation of EBV genomes in *Escherichia coli* (33), it has become feasible to restore the deleted region of the B95-8 strain using the equivalent DNA fragment of an EBV strain that retains the region. Here, we used BAC technology to seamlessly restore the missing 12-kb region at its native locus in a recombinant EBV B95-8 strain. We identified small but significant differences in the gene expression patterns of epithelial cells harboring recombinant viruses with or without the 12-kb deletion. We present genetic evidence here that multiple BART miRNAs cooperatively downregulate an epithelial cell-specific metastatic suppressor protein.

MATERIALS AND METHODS

Cell culture. B95-8 is a lymphoblastoid cell line obtained by infection of marmoset monkey peripheral blood leukocytes with EBV (2). HEK293 cells are neuro-endocrine cells obtained by transformation of embryonic kidney cells with adenovirus (34), and they have been used as EBV-producer cells (35). B95-8 cells, HEK293 cells, and Burkitt's lymphoma-derived Akata cells (36) were maintained in RPMI medium (Sigma-Aldrich Fine Chemicals, St. Louis, MO) supplemented with 10% fetal bovine serum (FBS). AdAH cells (37, 38) were maintained in Dulbecco modified Eagle medium (Sigma) supplemented with 10% FBS. C666-1 cells (a gift from Kowk-Wai Lo) (39) was maintained in RPMI medium supplemented with L-glutamine (Life Technologies) and 10% FBS. PC-3 cells (JCRB cell bank) were maintained In F-12K medium (Life Technologies) supplemented with 7% FBS.

Cloning of EBV genome as BAC clones. An experimental strategy to clone B95-8 strain EBV genome into a BAC vector is essentially the same as previously described methods (35, 40), except that a targeting vector with different right and left homology arms was used to facilitate a subsequent reconstitution of the B95-8 deleted region. A targeting vector with enhanced green fluorescent protein (EGFP) and hygromycin resistance genes (40), flanked by a right homology arm from the NheI site (nucleotide [nt] 143210) to the MluI site (nt 149732) of B95-8 strain EBV genome (V01555) and a left homology arm (from the BssHII site [nt 146953] to the NheI site [nt 154909]) was constructed. B95-8 cells were transfected with a NheI-linearized targeting vector, selected by hygromycin, and hygromycin-positive cell clones were obtained. Episomal fractions (41) of 14 hygromycin-resistant, EGFP-positive cell clones were used to transform electrocompetent DH10B cells. Bacterial colonies were obtained from 6 of 14 clones, and DNA minipreparation of 6 bacterial clones revealed that 2 of 6 clones were homologously recombined clones.

B95-8 cells harboring homologously recombined EBV-BAC clones were induced to productive replication by transducing BZLF1 (a switch gene of productive replication), and culture supernatants containing mixture viruses of parental B95-8 strain EBV and a targeted virus were used to establish lymphoblastoid cell lines (LCLs). EBV-BAC clones were subsequently rescued from the established LCLs, and an EBV-BAC clone with fewer (five copies) BamHI W repeats was selected. The estimated size of the obtained EBV-BAC clone, referred to as B95-8 EBV-BAC here, was ~169.5 kb.

Recombinogenic engineering to restore the B95-8 deleted region. Counter selection BAC modification kit (Gene Bridges, Dresden, Germany), a rapid homologous recombination system in *Escherichia coli*, was used to obtain a BART-restored EBV-BAC clone. A double-stranded DNA fragment containing kanamycin resistance and streptomycin sensitivity genes (rpsLneo) was amplified using primers listed in Table S1 in the supplemental material. A PCR product with 50-bp sequences homologous to subgenomic regions flanking the deletion junction (nt 152012) was obtained. The PCR product was inserted into the B95-8 deletion junction of the B95-8 EBV-BAC to obtain the intermediate clone by using neo as a positive selection marker. A DNA fragment of Akata strain EBV (36) was then used to restore the B95-8 deleted region. A part of BamHI B1 fragment (the MluI-BamHI subfragment, corresponding to nt 137443 to 146422 of EBV-wt) and an entire BamHI W1I1 fragment (corresponding to nt 146422 to 148949 of EBV-wt), both derived from Akata strain EBV, were tandemly cloned into pMBL19 vector (42) to obtain pMBL19 B/B1ΔW1I1. The rpsLneo gene of the intermediate clone was replaced with a BbvCI fragment of pMBL19 B/B1ΔW1I1 using rpsL as a negative selection marker. Bacterial colonies that were resistant to chloramphenicol and streptomycin were screened to obtain BAC clones that lost the rpsLneo cassette. As a result, the B95-8 deleted region was seamlessly restored in the BART(+) EBV-BAC. The sequence file of BART(+) EBV-BAC has been assembled from sequences of EBV B95-8 genome (V01555) (3) and the Family of Repeats (AJ278309) (43), EBV Akata sequence spanning the B95-8 deleted region (unpublished), and the transgenes (BAC vector and EGFP and hygromycin resistance genes) as shown in the supplemental material.

To generate a BART-deleted revertant, the rpsLneo PCR product described above was used to replace the 12-kb region of the BART(+) EBV-BAC with rpsLneo by using neo as a positive selection marker. A DNA fragment spanning nt 151912 to 152118 of B95-8 strain EBV was PCR amplified using the primers listed in Table S1 in the supplemental material. The obtained PCR product was subsequently used to replace the rpsLneo cassette by using rpsL as a negative selection marker.

To generate recombinant viruses with specific BART miRNA(s) deleted, rpsLneo was PCR amplified using the primers listed in Table S1 in the supplemental material, and a pre-miRNA gene of BART22 was first replaced by the rpsLneo cassette to obtain an EBV-BAC clone, BART22-rpsLneo. A double-stranded 120-bp PCR product, consisting of 60-bp upstream and 60-bp downstream sequences flanking the BART22 pre-miRNA sequence, was obtained by using oligonucleotides listed in Table S1 in the supplemental material. The rpsLneo of cassette of BART22-rpsLneo was replaced by the 120-bp PCR product to obtain a BAC clone of BART22Δ with no selective marker left behind. A similar experimental strategy was used to obtain EBV-BAC clones of BART8-11Δ and BART21-14Δ by using BART22-rpsLneo as a starting material. Primers used to make these recombinant genomes and to verify the deletions are listed in Table S1 in the supplemental material.

Recombinant virus production and infection. EBV-BAC DNAs were prepared from each 200-ml bacterial culture by using a Nucleobond BAC100 kit (Macherey-Nagel, Duren, Germany). HEK293 cells were transfected with BAC clone DNAs (1 μg of each) using Lipofectamine 2000 (Invitrogen). At 2 days posttransfection, the transfected cells were replated to 10-cm collagen-coated dishes in medium containing 150 μg of hygromycin per ml. Hygromycin-resistant colonies with bright EGFP fluorescence were grown, and cell clones that were highly competent for entering lytic replication after BZLF1 transfection were selected. Recombinant virus production was performed as described previously (40).

A retroviral vector pCLMFG-CR2, encoding EBV receptor CR2 (CD21), was constructed by inserting a PCR-amplified CR2 gene into pCLMFG-MCS vector, and VSVG-pseudotyped retroviral vector was produced as described previously (44). AdAH and PC-3 cells were infected with the retroviral vector expressing CR2 and were subsequently infected with either the recombinant viruses. Pools of stably infected AdAH and PC-3 cells were obtained by hygromycin selection. Lymphoblastoid cell lines (LCLs) were established by infecting peripheral blood mononuclear cells with the recombinant viruses as described previously (40).

miRNA expression analyses. Total RNAs were isolated from various cells using TRIzol reagent (Invitrogen) according to the manufacturer's instructions. For Northern blot analyses, aliquots (5 μg) of RNAs were electrophoresed through 15% polyacrylamide-urea gels, and separated RNAs were transferred onto Hybond N+ membrane (Amersham). Radiolabeled oligonucleotide probes specific for EBV miRNAs were prepared by end labeling of synthetic oligonucleotides with [γ-^{32}P]ATP (Perkin-Elmer Life & Analytical Sciences). Sequences of oligonucleotide probes are listed in Table S2 in the supplemental material. Membranes were prehybridized in ULTRAhyb-Oligo buffer (Ambion) at 37°C for 30 min, followed by hybridization with radiolabeled oligonucleotide probes at 37°C overnight. Membranes were washed with 2× SSC (1× SSC is 0.15 M NaCl plus 0.015 M sodium citrate) containing 0.05% sodium dodecyl sulfate (SDS) for 30 min at room temperature and then twice with 0.1× SSC containing 0.1% SDS for 15 min at room temperature. Signals were detected by means of BAS2500 analyzer (Fuji Film Inc.). For relative quantification of BART miRNAs in the infected cells, aliquots (100 ng) of RNAs were subjected to TaqMan small RNA assay (Applied Biosystems) (45) according to the manufacturer's instructions.

Cellular gene expression analyses. Total RNAs of two independent B95.8v-infected and two independent BART(+)v-infected HEK293 cell clones (or two independent pools of the infected AdAH cells) were processed for Microarray analysis using 3D-Gene human Oligo Chip 25k (Toray, Tokyo, Japan). cDNA synthesis, antisense RNA (aRNA) amplification, Cy5 labeling of aRNA, and hybridization to oligonucleotide tips were performed according to the supplier's protocol (3D-Gene; Toray). Hybridization signals were scanned using 3D Gene Scanner 3000 (Toray). The raw data for each spot were normalized by substitution with the mean intensity of the background signal. The detected signals for each gene were normalized by a global normalization method (the median of the detected signal intensity was adjusted to 25).

Quantitative reverse transcription-PCR (RT-PCR) analyses were performed by using the One-Step SYBR PrimeScript RT-PCR Kit II (TaKaRa Bio, Inc., Otsu, Japan) according to the manufacturer's instructions. Primer pairs used for NDRG1 and GAPDH cDNA amplification are listed in Table S3 in the supplemental material.

Western analyses. Aliquots of cells (4×10^6 cells each) were pelleted, resuspended in 150 μl of phosphate-buffered saline (without magnesium and calcium) and 300 μl of 1.5× lysis buffer (187.5 mM Tris-HCl [pH 6.8], 4.5% SDS, 9% urea, and 15% glycerol), and sonicated to obtain whole-cell extracts. Protein concentrations of the extracts were determined by using a DC protein assay kit (Bio-Rad). The equal aliquots of the extracts were electrophoresed through or SDS–10% polyacrylamide gels (for NDRG1, GAPDH, LMP1, and LMP2A) or SDS–7% polyacrylamide gels (for EBNAs) and subjected to Western blot analyses. Expressions of NDRG1 and GAPDH were detected by using either anti-NDRG1 rabbit monoclonal antibody D8G9 (Cell Signaling, catalog no. 9485) or anti-GAPDH antibody 14C10 (Cell Signaling, catalog no. 2118) as primary antibodies and a horseradish peroxidase-conjugated anti-rabbit IgG (GE Healthcare) as a secondary antibody. Expression of EBNAs was detected with human serum reactive to six EBNAs as a primary antibody and a horseradish peroxidase-conjugated anti-human IgG as a secondary antibody. The expression of LMP1 was detected using monoclonal antibody (MAb) S12 (specific to LMP1) and peroxidase-conjugated anti-mouse IgG, whereas the expression of LMP2A was detected using rat MAb 15F9 (Abcam) and peroxidase-conjugated anti-rat IgG.

Reporter assay and miRNA mimic transfections. Primer sequences used for making various NDRG1-related constructs are listed in Table S3 in the supplemental material. The 3′ untranslated region (UTR) of the NDRG1 gene was amplified by using genomic DNA of HEK293 cells as a template. The PCR product was digested by SpeI and cloned between SpeI-PmeI sites of pMIR-report (Ambion) to obtain pMIR-luc-NDRG1. NDRG1 cDNA was PCR amplified using pINCY-NDRG1 (Incyte cDNA Collection, clone LIFESEQ7593133; Thermo Scientific) as a template. The EcoRI-BamHI-digested PCR product was cloned into EcoRI-BglII-digested pSG5 vector (Stratagene) to make pSG5-NDRG1. A PCR-based mutagenesis protocol (46) was used to simultaneously introduce PstI sites to disrupt three BART22 seed-matched sequences within NDRG1 the 3′ UTR of pMIR-luc-NDRG1 (see Table S3 in the supplemental material).

Synthesized mirVana miRNA mimics of BART miRNAs were purchased from Applied Biosystems. For each well of 48-well dishes, the B95.8v-infected HEK293 cells (5×10^4 cells) were cotransfected with pMIR-luc-NDRG1 (2.5 ng), pRL-TK (1 ng), and 6 pmol of miRNA mimics (6 pmol/300 μl = 20 nM) by using Lipofectamine RNAiMAX (Invitrogen) according to an RT protocol. Triplicate transfections were performed for each sample. At 48 h posttransfection, cells were lysed by 1× passive lysis buffer (Promega) using 65 μl of per each well, and 20-μl aliquots were assayed by using a dual-luciferase reporter assay system (Promega) and a MicroBeta^2 LumiJET (Perkin-Elmer).

Immunohistochemistry and EBER-ISH of NPC biopsy specimens. Biopsy specimens were obtained from NPC patients who had been diagnosed at the Division of Otolaryngology at Kanazawa University Hospital, as well as its branch hospitals, according to protocols approved by the institutional review board. The data were analyzed anonymously. Paraffin-embedded specimens were used for the immunohistochemical analysis of NDRG1 (using anti-NDRG1 antibody; Cell Signaling, catalog no. 9485), as well as for EBER-ISH, as previously described (47).

RESULTS

Restoration of the 12-kb deleted region of the EBV B95-8 strain. The 12-kb genomic region that is deleted in the EBV B95-8 strain spans nt 139724 to 151554 of the EBV-wt sequence (NC_007605.1) (48). In the B95-8 strain (GenBank V01555), the deletion is located at nt 152012 (Fig. 1A). Notably, 17 of the 22 BART pre-miRNA genes are encoded within the deleted region (Fig. 1B).

The entire genomic sequence of the EBV B95-8 strain was cloned into a targeting vector containing a BAC vector sequence, a hygromycin resistance gene, and an enhanced green fluorescent protein expression cassette (Fig. 1A). The insertion sites of the transgenes differed from those of the previously described EBV-BAC clones 2089 (35) and 172-kb BAC (40) (Fig. 1A). Different insertion sites were chosen to facilitate the subsequent restoration of the 12-kb B95-8 deleted region. A B95-8 EBV-BAC clone with 5 copies of BamHI W repeat (~169.5 kb in size) was obtained (Fig. 1C). The clone with five BamHI W repeats was intentionally chosen (see Materials and Methods for details), as it should be small enough to accommodate a 12-kb additional sequence of the BART miRNA region later.

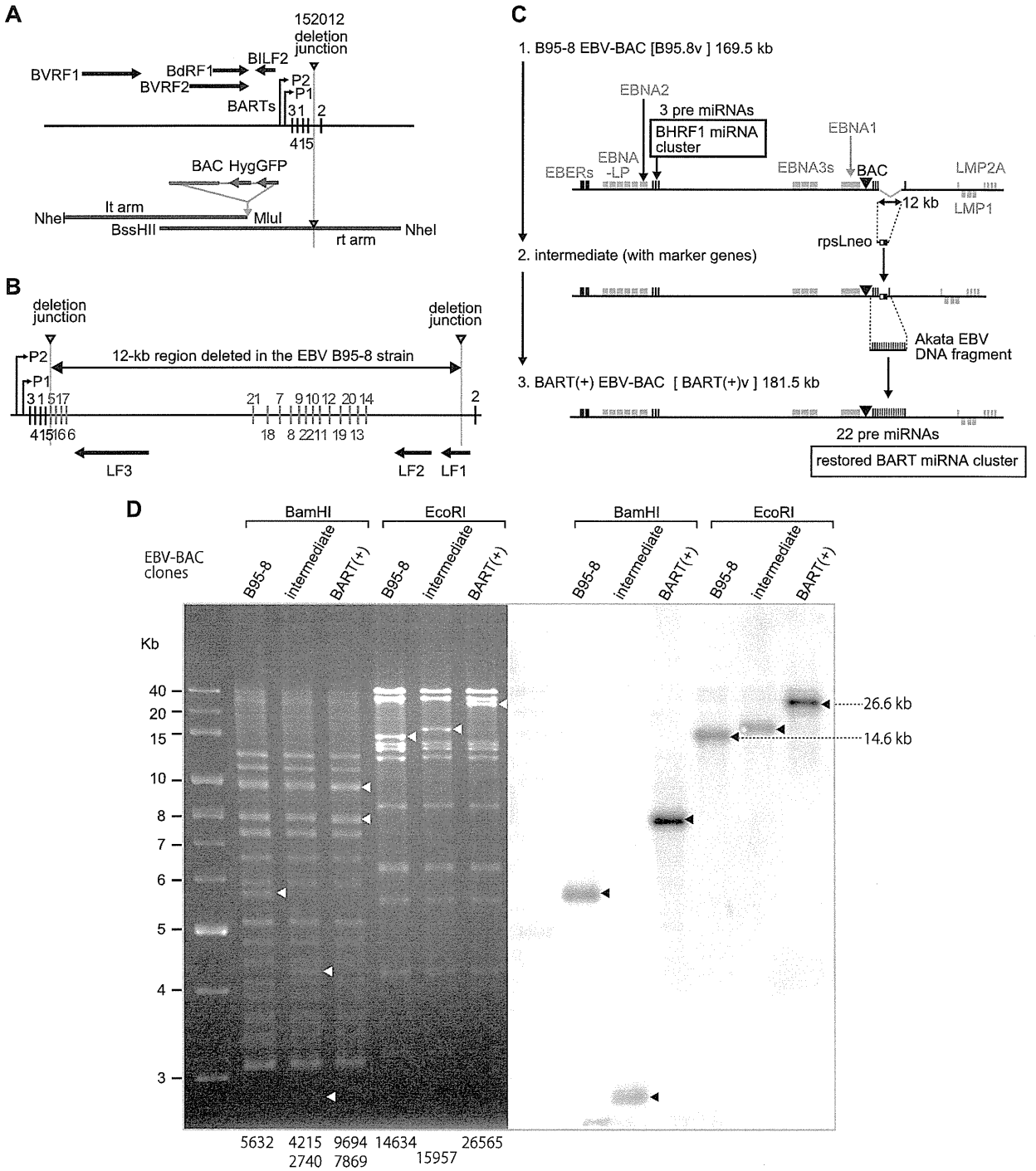

FIG 1 Experimental strategy used to restore the deleted BART miRNA cluster in the EBV B95-8 strain. (A) Schematic map of the deletion junction of the EBV B95-8 strain. The deletion junction is indicated with nucleotide no. of the B95-8 genome (V01555). The left (lt) and right (rt) homologous arms of the targeting vector and the restriction enzymes used to construct the vector are indicated. The viral open reading frames (horizontal arrows), BART transcription start sites (P1 and P2), and positions of the BART pre-miRNA genes (numbered vertical lines) are also shown. (B) Schematic map of the 12-kb region of EBV-wt that is missing in the EBV B95-8 strain. The numbered vertical lines indicate the positions of the pre-miRNA genes; those that are deleted in the EBV B95-8 strain are shown in gray. The horizontal arrows indicate the positions of viral open reading frames. (C) Schematic illustrations of the B95-8 EBV-BAC and the BART(+) EBV-BAC. The latter was obtained from the former via the intermediate clone with positive and negative selection marker genes (rpsLneo). A DNA fragment of EBV Akata strain was used to restore the missing 12-kb region of B95-8 EBV-BAC. (D) Restriction enzyme mapping and Southern blot analyses of the B95-8 and the BART(+) EBV-BAC clones. The intermediate clone was also included to the analysis. The DNAs were digested with BamHI or EcoRI and analyzed by agarose gel electrophoresis followed by ethidium bromide staining (left panel). The BamHI and EcoRI fragments spanning the deletion junction are indicated by arrowheads, and their calculated sizes (see Table S4 in the supplemental material for the details) are indicated at the bottom. The gel was subsequently processed for Southern blot analysis (right panel) using the BamHI W1I1 fragment of the EBV Akata strain as a probe. Note the 12-kb increase in the size of the EcoRI fragment spanning the deletion junction in the BART(+) EBV-BAC clone.

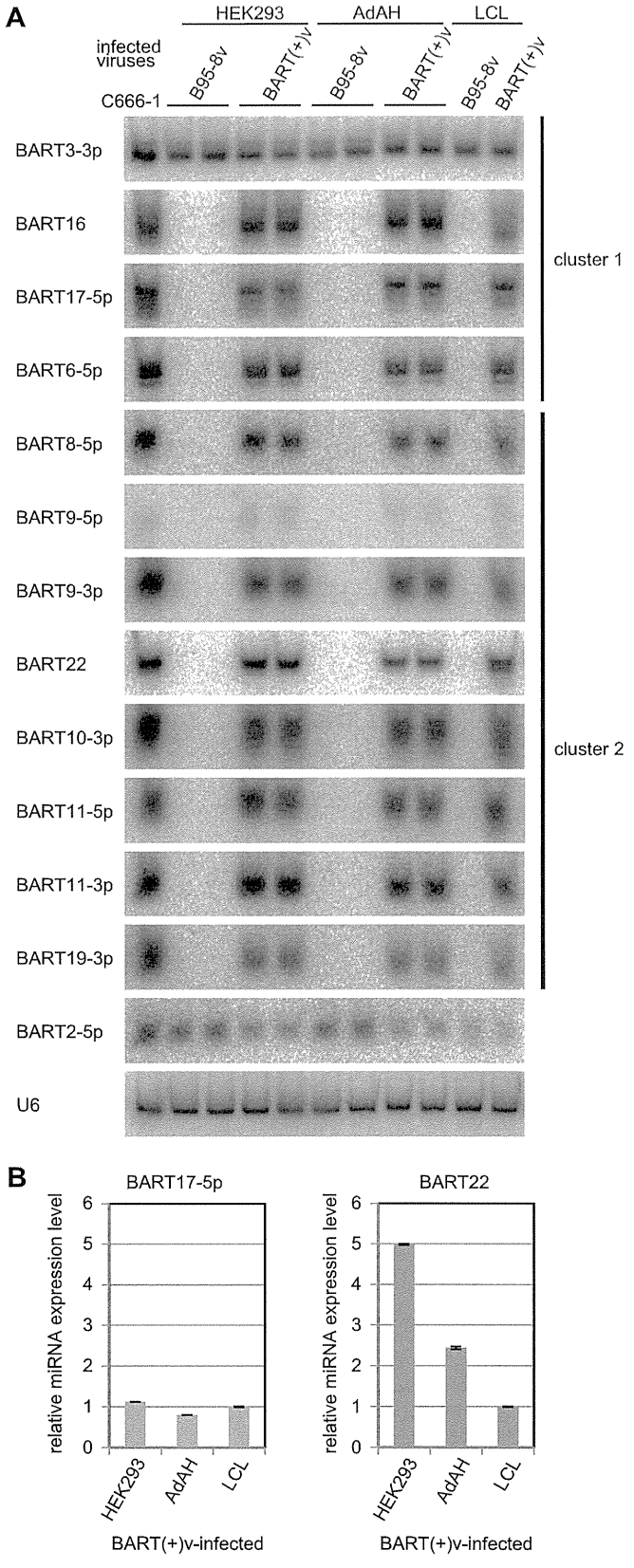

FIG 2 Expression of BART miRNAs in the cells infected with the recombinant viruses. (A) The expression levels of 13 BART miRNAs (four from cluster 1 and eight from cluster 2) in the B95.8v-infected and the BART(+)v-infected HEK293 cells, AdAH cells, and LCLs were examined by Northern blotting. Total RNA extracted from the NPC-derived C666-1 cell line was used as a control. The expression of U6 snRNA was used as a loading control. (B) TaqMan small RNA assay was used to determine relative expression levels of BART17-5p and BART22 in the BART(+)v-infected HEK293 cells, AdAH cells, and LCLs. The values of miRNA expression levels were normalized by those of hsa-miR-16 expression levels among different cells. The average miRNA expression levels in the LCLs were adjusted to 1.

The obtained BAC clone was further modified using *E. coli*-mediated recombinogenic engineering. First, tandemly connected positive and negative selection marker genes were inserted to the B95-8 deletion junction to obtain an intermediate clone (Fig. 1C). Subsequently, the DNA fragment of the EBV Akata strain (36), which is a type 1 EBV, like the B95-8 strain, was used to replace the marker genes of the intermediate clone. The BART-restored EBV-BAC clone, designated BART(+) EBV-BAC (Fig. 1C), was ~181.5 kb in size, which is within the size limits for efficient packaging into virions (49). Restriction enzyme mapping and Southern blot analyses of the repaired region confirmed the expected 12-kb increase in the sizes of bands spanning the repaired region (Fig. 1D and see Table S4 in the supplemental material).

Establishment of cell lines infected with the B95-8 or the BART-restored virus. To generate virus-producing cells, the newly obtained B95-8 and BART(+) EBV-BAC clones were stably transfected into HEK293 cells, and multiple HEK293-derived cell clones capable of producing recombinant viruses [here referred to as B95.8v and BART(+)v] were obtained. The integrity of the EBV genomes in the stably transfected HEK293 cell clones was confirmed by recovering the BAC clones from the cells and subjecting them to restriction enzyme analyses (data not shown). The obtained virus-producing HEK293 cells are here referred to as "B95.8v-infected" and "BART(+)v-infected" HEK293 cells. Frozen virus stocks of B95.8v and BART(+)v with up to $10^{4.5}$ CFU/ml transforming titers were obtained and used for infection experiments.

For epithelial cell infection, AdAH cells were chosen as recipient cells. The AdAH cells had long been assumed as human adenoid epithelium-derived cells (38). However, they are likely to be contaminated with human cervical carcinoma-derived HeLa cells (37), as they were actually positive for human papillomavirus type 18 DNA and E6 E7 mRNA expression (data not shown). AdAH cells were transduced with the EBV receptor CR2 (CD21) and then infected with the viruses. Pools of stably infected AdAH cells were obtained by hygromycin selection. Multiple LCLs were also established by infecting peripheral B lymphocytes with the viruses.

Total RNAs were extracted from the infected HEK293 and AdAH cells, as well as from the LCLs, and the expression levels of 13 BART miRNAs were examined by Northern blotting (Fig. 2A). The total RNA of the EBV-positive NPC cell line C666-1 (39) was used as a positive control. BART3-3p and BART2-5p, which are encoded upstream and downstream of the B95-8 deleted region, respectively, were expressed in all of the cell types. Notably, BART2-5p expression was enhanced slightly in the B95.8v-infected cells, presumably because the BART2-5p gene was located near the BART transcription start site due to the 12-kb deletion (Fig. 1B).

As expected, all of the BART miRNAs that are encoded within the B95-8 deleted region (16, 17-5p, 6-5p, 8-5p, 9-5p, 9-3p, 22, 10-3p, 11-5p, 11-3p, and 19-3p) were expressed only in the cells that were infected with the BART-restored virus (Fig. 2A). BART9-5p and BART20-5p were hardly expressed in all of the